Amorphization and Characteristics of Shapes of Comminuted

Particles Formed in Comminution Process

that Accompanied Fault Movement:

An Approach by Comminution Experiments

February   2012

Kana   OZAWA

Amorphization and Characteristics of Shapes of Comminuted

Particles Formed in Comminution Process

that Accompanied Fault Movement:

An Approach by Comminution Experiments

Kana   OZAWA

CONTENTS

Part 1   Amorphous material formed by the mechanochemical effect in natural pseudotachylyte of crushing origin:

A case study of the Iida-Matsuka Fault, Nagano Prefecture, Central Japan

Part 2 Differentiation and origin of the amorphous materials in pseudotachylyte revealed by transmission electron microscopic observations

Part 3 Amorphization of biotite reproduced in the comminution experiment using a mechanical agate mortar

Part 4 Microstructures of the sliding surfaces formed in crush-origin pseudotachylyte, at high and low slip rates determined by shapes of submicron comminuted particles

Abstract

This study has focused on shape-characteristics and amorphization of the particles formed during the comminution process accompanied by fault movement and reported by some comminution experiments for the following four purposes.

The natural crush- origin pseudotachylyte was described down to the nanometer scale, of which the observations were explained by the process to form the comminuted particles reproduced by comminution experiments.

(1) Amorphous material formed by the mechanochemical effect in natural pseudotachylyte of crushing origin: A case study of the Iida-Matsukawa Fault, Nagano Prefecture, Central Japan

Pseudotachylytes from the Iida-Matsukawa Fault, Central Japan (Iida pseudotachylytes), are described down to the nanometer scale using high-resolution electron microscopy, scanning electron microscopy (SEM), analysis of chemical compositions, and mercury intrusion porosimetry. The pseudotachylyte matrix chiefly consists of the nanoscale particles and elongated submicron fragments of biotite composition; amorphous material of several tens of nanometers in size is also observed, despite the absence of melt textures. Lattice fringe images reveal that the amorphous phase coexists with lattice distortion in deformed biotite fragments that are several hundreds of nanometers in size. The presence of these submicrostructures indicates that the amorphous material formed by mechanical stress during the comminution process; that is, via the "mechanochemical effect." We conclude that amorphous material does not always provide evidence of the rapid cooling of melt in pseudotachylyte. The

amorphous materials present in the Iida pseudotachylyte resulted from the mechanochemical effect due to both shear stress and normal stress during the comminution process accompanied by fault motion.

(2) Differentiation and origin of the amorphous materials in pseudotachylyte revealed by transmission electron microscopic observations

Amorphous materials in pseudotachylyte from the Hatagawa Fault Zone (HFZ) in Fukushima Prefecture were analyzed using by transmission electron microscope (TEM). The pseudotachylyte matrix includes amorphous materials which have both irregular shapes and uniform contrast in bright-field images. Their appearances in the TEM images are distinct from those of the amorphous nanoparticles in the crush-origin pseudotachylyte from the Iida-Matsukawa Fault (IMF) in Nagano Prefecture. Melting experiments were performed on the host rock for the pseudotachylyte from HFZ and low-speed shear tests of the host rock for the pseudotachylyte from IMF, producing the amorphous materials in each experiment. The TEM images also reveal the amorphous materials to have different characteristics. It is suggested that the origin of amorphous materials in pseudotachylyte can be distinguished by their appearance in the TEM images.

(3) Amorphization of biotite reproduces in the comminution experiment using a mechanical agate mortar

The experiment on comminution of natural biotite was conducted using a mechanical agate mortar. X-ray diffraction (XRD) and transmission electron microscope (TEM) analyses revealed that the particles had an amorphous pattern after grinding for

312 hours. SEM and TEM observations showed that the amorphous materials formed were spherical particles 100 nm in diameter. Infrared spectroscopy analyses indicate that the absorption indicating Si-O-Si stretching vibration broadened after grinding for 48hours, and the XRD analyses showed that the (060) reflection had disappeared. There were therefore disturbances in the structural link between the tetrahedral and octahedral layers. Furthermore, infrared spectroscopic analysis after 120 hours grinding showed absorption indicating that the Si-O-Fe bonding had broadened, and the most intense XRD peak had disappeared. These results suggested that disturbance had occurred in the oriented layer structure of the biotite's c-axis. The biotite therefore changed from single crystals to amorphous materials by comminution, not melting.

(4) Microstructures of the sliding surfaces formed in crush-origin pseudotachylyte, at high and low slip rates determined by shapes of submicron comminuted particles

We performed sliding shear tests at two slip rates: 1 or 5 cm of displacement at <1 cm/s (high-speed conditions) and 1 cm of displacement at ~1 cm/30 min (low-speed conditions). We then investigated the conditions of formation of amorphous particles in the pseudotachylytes of the Iida–Matsukawa fault. The shapes of submicron comminuted particles differed markedly depending on the slip rate conditions. At the high slip rate, most particles were elongated, whereas at the low slip rate the particles were polygonal or spherical. These results were true for all sample types (i.e. quartz, biotite, and granite cataclasite which the host rock of the Iida–Matuskawa pseudotachylyte).

In the Iida–Matsukawa pseudotachylyte, the elongated submicron particles in the shear planes that were the most parallel to the pseudotachylyte vein were aggregated. In contrast, the particles in the shear planes that were about $30°$ oblique to the vein were dispersesd and were polygonal or nearly spherical.

On the basis of the above sliding shear tests, the former shear planes form under high slip rates, whereas the latter form under low slip rates. Consequently, the sliding surfaces formed at high and low slip rates could be distinguishable in the shapes of the submicron-sized comminuted particles in fault rocks.

List of Figures

List of Table

Part 1 Amorphous material formed by the mechanochemical effect in natural pseudotachylyte of crushing origin: A case study of the Iida-Matsukawa Fault, Nagano Prefecture, Central Japan

1. Introduction

Pseudotachylytes are fault rocks that are generally thought to form by frictional fusion and comminution during paleoseismic fault movements (e.g., Philpotts, 1964; Sibson, 1975; Allen, 1979). Although it has been debated in the past as to whether pseudotachylyte matrix originates from frictional fusion or comminution (Wenk, 1978), the controversy was resolved by Spray's (1995) experimental study undertaken using friction welding apparatus, which demonstrated that comminution is a necessary precursor to frictional melting.

Pseudotachylytes are now generally divided into melt-origin types and crush-origin types. Melt-origin types contain melt textures such as glass or glassy material, spherulites, dendritic microlites, vesicles, amygdules, rounded and embayed clasts, and sulfide blebs (e.g., Philpotts, 1964; Sibson, 1975; Allen, 1979; Maddock, 1983, 1986; Maddock et al., 1987; Magloughlin, 1989, 1992, 2005; Lin, 1994, 1999). Melt-origin pseudotachylytes from the Fuyun Fault zone, China, have a largely glassy matrix that is nearly isotropic and variable in color from colorless to grey, brown, and yellowish-brown, as well as containing flow streaks (Lin, 1994).

In contrast, crush-origin types show none of these melt textures. Such pseudotachylytes have been described from the Iida-Matsukawa Fault, Japan (Lin et al., 1994; Lin, 1996, 1997b), the Nojima Fault, Japan (Shigetomi and Lin, 1999; Lin et al.,

2001), and the Shimotsuburai Fault (Kano et al., 2004), part of the active fault system of the Itoigawa-Shizuoka Tectonic Line, Japan.

Glass and other amorphous material are known to form not only via the rapid cooling of melt, but also by alteration (e.g., Henley and Ellis, 1983) and comminution (e.g., Kubo, 1963; Kubo and Miyazaki, 1968; Kieffer *et al.*, 1976; Lin and Nadiv, 1979; Sakabe *et al.*, 1998). The results of rotary shear sliding experiments using samples of granite and quartzite have shown that the amorphous silica formed by comminution on a sliding surface can be observed by transmission electron microscopy (TEM) (Yund *et al.*, 1990). Most recently, Goldsby and Tullis (2002) and Di Toro *et al.* (2004) reported an extraordinary progressive reduction in frictional resistance upon sliding surfaces under wet conditions at subseismic slip rates. The authors explained this weakening as resulting from amorphization and the formation of gel via shearing and comminution in the presence of water, and suggested this to be one of the weakening mechanisms of faults during seismic slip.

The above experimental studies clearly show that the presence of amorphous material formed by comminution is an essential factor in understanding fault strength and faulting processes during earthquakes; however, the presence of amorphous material formed by comminution has yet been reported from natural fault rocks.

The present study describes submicron-scale textures observed via electron microscopy and comminution-origin amorphous material revealed by TEM analyses of crush-origin pseudotachylyte from the Iida-Matsukawa Fault, southern Nagano Prefecture, Central Japan (Iida pseudotachylyte). We propose that the amorphous material within the Iida pseudotachylyte formed via mechanochemical effects rather than rapid cooling of the melt during seismic faulting.

2

2. Sample locality

The Iida-Matsukawa Fault strikes NW–SE and dips 75–85° to the SW, extending for 12 km in the southern part of the Kiso Range, Central Japan (Fig. 1). Geological and topographical evidence indicates that the fault is an active sinistral strike-slip fault with a component of normal dip-slip displacement, having a horizontal slip rate of 1 mm/y (Lin *et al.*, 2000).

Lin *et al.* (1994) and Lin (1996, 1997a, b) described in detail the field occurrence of pseudotachylytes and cataclastic rocks from along the Iida-Matsukawa Fault. The zone of fractured rock along the fault generally ranges in width from several meters to several tens of meters, and consists of cataclastic rocks such as cataclasite, foliated cataclasite, fault breccia, fault gouge, and pseudotachylyte (Lin, 1996, 1997a, b). The pseudotachylyte veins observed along the fault are several millimeters to several centimeters wide, dark brown to black in color (Fig. 2b), locally show a vitreous luster, and occur both as simple veins along the main fault plane (fault veins) and as complex networks of veins (injection veins; Fig. 2a) within host granitic cataclasite (Lin *et al.*, 1994; Lin, 1996, 1997a, b).

The granitic cataclasite, the host rock of the pseudotachylyte, occurs along the main fault plane in a zone that ranges in width from several tens of centimeters to several tens of meters (Lin *et al.*, 1994). The host rock is largely composed of quartz, feldspar, and biotite (Lin, 1997a). In places, the cataclasite contains a well-developed foliation that dips at 25–35° to the SE, subparallel to the main fault plane. The foliation is defined by the preferred orientation of biotite clasts and aggregates of quartz grains and feldspar porphyroclasts. Deformed biotite in the cataclasite shows cleavage steps, mica "fish" geometries, and kink bands, indicating a sinistral sense of shear (Lin, 1996,

1997a; Lin *et al.*, 2000).

The pseudotachylyte analyzed in the present study was collected from a fault vein in an outcrop that corresponds to Location 2 of Lin *et al.* (1994) and Lin (1996), located along the central segment of the Iida-Matsukawa Fault at the southernmost part of Tsunbodaira, along the Matsukawa River in Iida City (Fig. 1).

3. Analytical methods

Microstructures in the pseudotachylyte were observed using a JEOL JSM-6320F high-resolution scanning electron microscope (HRSEM) with an accelerating voltage of 5 kV, a JEOL JEM-100CX TEM with an accelerating voltage of 100 kV, and a JEOL JEM-2100 high-resolution transmission electron microscope (HRTEM) with an accelerating voltage of 200 kV. The freeze-dried breakage surface of the pseudotachylyte was investigated by HRSEM. Foils for TEM observations of microstructures in the pseudotachylyte were prepared from thin sections, without epoxy resin, using an ion-beam. Samples for HRSEM and TEM observations of particles smaller than 2 μm were prepared as follows. Untreated lumps of the pseudotachylyte were suspended in distilled water using ultrasonic agitation; the < 2 μm fractions were then selected by hydraulic elutriation. The same suspension was dropped onto a microgrid (without films) subjected to hydrophilic treatment for TEM observations. Samples for HRSEM analysis were covered with platinum, while TEM specimens were carbon-coated.

X-ray diffraction (XRD) patterns of the pseudotachylyte and host granitic rock were obtained using a RINT RAD-C X-ray diffractometer operated under the following analytical conditions: filtered Cu-Kα radiation, X-ray generator at 40 kV, 25 mA,

4

scanning step 0.02°, scanning speed 2°/min, divergence slit 1°, scattering slit 1°, and receiving slit 0.15 mm. Powdered samples for XRD analysis, analyzed to identify clay minerals, comprised the < 2 μm fractions selected by hydraulic elutriation and prepared as well-oriented aggregates on a silica glass slide. The treatments used in this study were as follows. Individual samples were heated to either 150, 350, 450, 550, or 600 °C for 1 hour, followed by quenching in air and treatment with ethylene glycol.

The bulk chemical compositions of the pseudotachylyte and host rock were determined via the analysis of whole-rock powder samples using a JSX-3220 energy-dispersive X-ray fluorescence spectrometer (XRF-EDS). The powder sample of pseudotachylyte for XRF-EDS analysis was selected, as much as possible, from only black veins of pseudotachylyte, as viewed under the microscope.

The chemical composition of the pseudotachylyte matrix was determined from carbon-covered specimens, polished thin sections, and foils for TEM analysis. The thin sections were examined using a JEOL JSM-5600LV scanning electron microscope (SEM) operating at 15 kV with an energy-dispersive X-ray spectrometer (EDS). The foils for TEM analyses were examined using a JEOL JEM-2100 HRTEM with a 200 kV accelerating voltage and fitted with an EDS.

The pore-size distributions of freeze-dried specimens of the pseudotachylyte and host rock were determined using a Shimadzu-Micromeritics AutoPore IV-9520 mercury porosimeter. This method is capable of determining pore sizes ranging from 0.003 to 180 μm.

4. Microstructures

4.1. Optical observations

The pseudotachylytes investigated in this study contain angular clasts of quartz and feldspar within a dense fine-grained matrix that is pale to dark brown under plane-polarized light (Fig. 3a, b). The boundary between the pseudotachylyte and host rock (granitic cataclasite) is generally sharp (Fig. 3a). Pseudotachylyte veins cut across deformed biotite in the host rock, which is elongated and contains kink bands (Fig. 3c, d); however, few fragments of biotite are observed in the pseudotachylyte itself. The pseudotachylyte matrix contains thin dark-brown layers that resemble flow structures (Fig. 3a). The pseudotachylyte contains no melt textures such as spherulites, dendritic microlites, vesicles, amygdules, rounded and embayed clasts, and sulfide blebs.

4.2. HRSEM observations

The pseudotachylyte matrix is relatively porous, and mainly characterized by extremely fine-grained aggregates that range in size from several tens of nanometers to a few micrometers (Fig. 4a–c). Most of the larger fragments of a few micronmeters in size, are angular to sub-angular and irregular in shape, with sharp or little-blunt edges and peaks. The fragments show conchoidal fractures and step-like textures on the surfaces. Most of the surface features are relatively smooth, without etch pits or deep cavities (Fig. 5a–d). Some fragments contain numerous small scratches and holes upon sub-rounded surfaces (Fig. 5b).

Roundness is an estimate of the degree of smoothness of a grain surface (e.g. Leeder, 1982), and the analyzed fragments show a low degree of roundness, approximately 0.2–0.3 according to the scheme of Krumbein (1941, Plate 1). The

6

smaller submicron fragments—several hundreds of nanometers in size—tend to have more spherical forms; however, they also have many corners on their surfaces, with relatively low roundness values of 0.3–0.4 (Fig. 5e–g). The surface textures of submicron fragments with blunt edges are slightly rough, without etch pits or deep cavities (Figs. 4b, 5e–g). The pseudotachylyte matrix does not contain melt textures such as stringy textures (e.g., Spray, 1989, 1995; Kennedy and Spray, 1992).

4.3. TEM observations

The pseudotachylyte matrix mainly consists of randomly oriented fragments that range in size from several tens of nanometers to a few micrometers; the minimum size is approximately 20 nm. The larger angular to sub-rounded fragments, which range in size from several hundreds of nanometers to a few micrometers, are generally isolated within the matrix, and supported by elongated fragments of several hundred nanometers in length and nanoscale particles smaller than 100 nm (Figs. 6a, 8a). The nanoscale particles have irregular tabular shapes (Figs. 7a, 8b), while the elongated fragments show evidence of gliding and are bent and torn along layer boundaries (Figs. 6c, 8c–e). Few euhedral particles are observed in the pseudotachylyte matrix.

The selected area diffraction (SAD) patterns obtained from 100 kV TEM observations of areas dominated by the elongated fragments and nanoscale tabular particles revealed the superimposition of diffuse ring patterns, ring patterns with biotite spacings, and several diffraction spots (Fig. 6b, c). This finding indicates that amorphous material coexists with very fine crystalline fragments in such areas of the pseudotachylyte, and that the fragments are randomly orientated. The SAD patterns were taken with an aperture of 500 nm diameter due to the limitations of the technique

employed by the 100 kV TEM. There is also the risk of amorphization arising from damage by the ion-beam when preparing specimens thinned by ion milling. To cope with these problems, fragments smaller than 2 μm were dispersed by ultrasonic agitation in distilled water, and the particles on the microgrids were then observed to verify the amorphous material more accurately, as shown in Fig. 7. SAD revealed that most of the angular to sub-rounded particles of several hundreds of nanometers in size have a single-crystal pattern (Fig. 7b), while agglomerations of nanoscale tabular particles show diffuse ring patterns (Fig. 7a).

Lattice fringe images of the deformed elongated fragments, as obtained using 200 kV TEM, revealed some lattice fringes with 1 nm spacings, with some of the spaces of the lattice fringes being non-periodic and indistinct (Fig. 8d–f). The above results indicate that the nanoscale tabular particles are amorphous material, whereas the deformed elongated fragments include amorphous phases and lattice distortion. The diffraction spots in the SAD patterns obtained by 100 kV TEM are probably derived from the larger grains (several hundreds of nanometers in size) adjacent to the smaller particles.

Biotite fragments were picked out of the host rock and observed by 100 kV TEM by placing them on a microgrid without a film. SAD revealed that most of the biotite fragments have single-crystal patterns (Fig. 7c).

5. X-ray diffraction patterns

The XRD patterns of the main minerals in the pseudotachylyte and host rock are shown in Fig. 9a. The pseudotachylyte consists of quartz, plagioclase, alkali feldspar, and a little clay mineral. No increased background is observed in the XRD patterns of

pseudotachylyte. The host rock consists of quartz, plagioclase, alkali feldspar, and clay mineral that include mica clay minerals. The XRD patterns of the clay minerals in the pseudotachylyte and host rock are shown in Fig. 9b and c, respectively. The clay minerals were identified according to Oinuma and Kodama (1967). The 7-Å reflections in both pseudotachylyte and host rock disappeared after heating at 550 °C, suggesting kaolinite. The 10-Å reflection in the host rock did not disappear after heat treatment, suggesting mica clay minerals, while the 14-Å reflections in both the pseudotachylyte and host rock shifted to 17 Å, suggesting montmorillonite. The pseudotachylyte contains fewer clay minerals than the host rock. Of note, the peaks of mica clay minerals were identified only in the host rock, not in the pseudotachylyte.

6. Chemical composition

Table 1 shows the bulk chemical compositions of the pseudotachylytes and host rock analyzed by XRF-EDS. Sampling points for the XRF-EDS analyses are shown in Fig. 2a. The pseudotachylytes have a slightly lower SiO_2 content and higher TiO_2, Fe_2O_3, and MgO contents than the host rock. Elemental maps obtained using SEM-EDS reveal that the pseudotachylyte matrix is particularly enriched in Mg, Ti, and Fe (Figs. 3b, 10).

The chemical compositions of particles smaller than 1 μm in the pseudotachylyte matrix were analyzed using TEM-EDS. Both the elongated fragments and the nanoscale tabular particles consist of Mg, Al, Si, K, Ti, and Fe. The C peaks detected by TEM-EDS analysis reflect contamination from the carbon coating (Fig. 11a, b).

7. Pore-size distribution

The results of pore-size analyses are shown in Fig. 12. The modal pore diameters of the pseudotachylyte and host rock are 0.0098 and 0.068 μm, respectively, while the total intrusion volumes are 0.026 and 0.040 ml/g. The porosity of the pseudotachylyte is 6.4%, whereas that of the host rock is 9.6%. These data clearly demonstrate that the host rock is more porous than the pseudotachylyte.

8. Discussion

8.1. Evidence for crush-origin pseudotachylyte

Based on optical microscopy and SEM observations, Lin *et al.* (1994) and Lin (1996) reported that pseudotachylytes from the Iida-Matsukawa Fault contain few melt textures, and that the matrix mainly consists of fine-grained angular fragments larger than 2–3 μm, indicating an origin via crushing rather than melting. Our own optical microscopy and HRSEM observations also reveal the absence of melt textures such as spherulites, dendritic microlites, vesicles, amygdules, sulfide blebs, and stringy textures. Previous studies have reported the results of SEM observations of quartz grains within granitic rocks subjected to triaxial compression tests (e.g., Krinsley and Doornkamp, 1973; Dengler, 1976; Kanaori *et al.*, 1980, 1982). These studies described quartz grains with angular shapes and sharp edges and peaks, exhibiting conchoidal fractures and step-like textures on the surfaces.

The fragments of a few micrometers in size in the Iida pseudotachylyte also show conchoidal fractures and step-like textures (Fig. 5a–c), indicating an origin via crushing; however, some of their edges and peaks are rounded (Fig. 5b), and the submicron fragments tend to be spherical in shape (Fig. 5e–g). Such rounded fragments have been

documented to form not only by melting but also by attrition wear (e.g. Chester *et al.*, 1993, 2003) and chemical dissolution in groundwater (e.g., Kanaori *et al.*, 1980, 1982; Kanaori, 1983). Chester *et al.* (1993) suggested that rounded fragments in ultracataclasites along the North Branch San Gabriel and Punchbowl faults formed via attrition wear as angular fragments rolled within the surrounding matrix. The shapes of particles of clay minerals and quartz, formed by prolonged grinding within a mechanical agate mortar, revealed to become rounded by TEM observations (e.g., Takahashi, 1959; Shimazu, 1962).

Kanaori et al. (1980, 1982) and Kanaori (1983) examined the surface textures of quartz grains from various fault gouges using SEM, and classified the surface textures of grains into four groups based on the degree of corrosion by groundwater. They showed that the features of the grains change gradually, with progressive corrosion, from irregular angular shapes and smooth surfaces to rounded shapes and rough undulatory surfaces with etch pits and deep cavities. Lin (1999) reported that fragments of > 10 μm in size that formed via melting have a high degree of roundness (> 0.4), whereas fragments that formed via attrition wear or chemical dissolution in groundwater have a low degree of roundness (< 0.4).

The fragments in the present pseudotachylyte of a few micrometers in size and with rounded edges and peaks are marked by small scratches and holes (Fig. 5b). These textures (similar to the abrasion pits reported by Baker, 1976; Fig. 2E), in combination with their low degree of roundness (0.2–0.3), suggest that the rounded edges and peaks originated via attrition wear. The degree of roundness of the submicron particles in the pseudotachylyte is also low (0.3–0.4), suggesting that the particles formed by processes other than melting. The submicron particles have slightly rough surfaces, without

textures such as abrasion pits (Fig. 5e–g). These textures are similar to the subconchoidal fracture and orange peel-like texture formed when particles are weakly affected by chemical dissolution in groundwater following fault movement (Kanaori *et al.*, 1980, 1982); however, the present pore-size distribution data indicate that most of the pores in the pseudotachylyte are smaller than 100 nm, and that the host rock is more porous than the pseudotachylyte (Fig. 12), thereby suggesting that fluid is unlikely to have passed through the pseudotachylyte subsequent to its formation.

The obtained XRD patterns reveal that the Iida pseudotachylyte contains fewer clay minerals than the host rock; moreover, most of the fragments have irregular shapes, and few euhedral particles were observed in the pseudotachylyte matrix. It is therefore inferred that the Iida pseudotachylyte is negligibly affected by chemical dissolution in groundwater and hydrothermal alteration subsequent to fault movement. We propose that most of the spherical submicron fragments formed by attrition wear during fault movement.

Flow structures were reported as melt textures in the melt-origine pseudotachylyte (e.g., Sibson, 1975; Berlenbach and Roering, 1992; Lin, 1994); however, they have also been reported from fluidized intrusive systems such as dikes and breccias, formed by the fluidization of solid particles (e.g., Fairbairn and Robson, 1942; Reynolds, 1954). Lin (1996, 1997b) also suggested that veins of Iida pseudotachylyte formed via the fluidization of crushed fine-grained material generated in the shear zone during seismic faulting. This interpretation was based on the similar bulk chemical compositions and grain-size distributions of injection veins and fault veins. Thus, the flow structures in the pseudotachylyte observed by optical microscope are likely to have formed by fluidization rather than the flow of a melt (Fig. 3a). On the basis of the facts presented

above, we conclude that the Iida pseudotachylyte is of crush origin rather than melt origin.

8.2. Formation of amorphous material

Naturally occurring amorphous material can form via the rapid cooling of melt, chemical weathering, hydrothermal alteration, and mechanochemical effects induced by mechanical energy during the comminution process. We strongly favor the latter process in considering the formation of amorphous material in the Iida pseudotachylyte, as explained in the following text.

It is well known that comminution induces solid-state phase transformations such as amorphization and polymorphic transformation, as well as changes in the physical and chemical properties of materials. These phenomena are termed "mechanochemical effects" (e.g., Kubo, 1963; Kubo and Miyazaki, 1968; Lin and Nadiv, 1979). The driving forces of solid-state phase transformations that take place during comminution processes such as crushing, grinding, pulverizing, and polishing, include strain energy, shear energy, thermal energy, sound energy, and kinetic energy (e.g., Lin *et al.*, 1975; Lin and Nadiv, 1979). Numerous studies report marked amorphization during the crushing or prolonged grinding of minerals, particularly quartz (e.g., Ray, 1923; De Carli and Jamieson, 1959; Shimazu, 1962; Lin and Somasundaran, 1972; Sakabe et al., 1998) and mica and clay minerals (e.g., Laws and Page, 1946; Mackenzie and Milne, 1953a, b; Yoder and Eugster, 1955; Takahashi, 1959; Perez-Rodriguez *et al.*, 1988). Extensive work on the grinding of clay minerals has led to the proposal that the structure of crystalline parts in the material becomes disordered due to mechanical stress such as shear stress and impact stress, ultimately changing into amorphous material (e.g.,

Takahashi, 1959).

Yund *et al.* (1990) reported the formation of amorphous material via comminution in granite gouges generated experimentally by rotary shear sliding. The authors stated that the amorphous material coexisted with very fine angular crystalline fragments with irregular boundaries, and that there appeared to be a continuum between the amorphous material and crystalline fragments. In addition, the amorphous material formed by comminution was distinct from the amorphous material formed by melting, which had sharp, distinct boundaries and uniform contrast in bright-field images (e.g., Dell'Angelo *et al.*, 1987).

In the present study, bright-field images of the pseudotachylyte matrix obtained from 100 kV TEM analyses also indicate that the amorphous material coexists with very fine crystalline fragments that range in size from several tens to several hundreds of nanometers. As described in the earlier studies, the fragments have irregular boundaries, and there appears to be a continuum between the amorphous material and crystalline fragments (Fig. 6b).

HRTEM images of the pseudotachylyte matrix reveal that elongated fragments with 1 nm spacings, corresponding to the (001) spacing of biotite, bend or glide parallel to the layers (Fig. 8d, e), suggesting mechanical stress. The amorphous phase coexists with lattice distortion within the deformed fragments (Fig. 8e, f), indicating that the amorphous phases in the elongated fragments formed due to mechanochemical effects induced by mechanical stress.

Nanoscale amorphous material smaller than 100 nm has been reported to form during chemical weathering and the hydrothermal alteration, such as primitive clay precursors, amorphous silica, allophone, imogolite, and ferrihydrite (e.g., Tazaki, 1986;

14

Marumo, 1995). Tazaki's (1986) HRTEM observations of weakly weathered feldspar revealed ultrathin amorphous material in 20–25 nm circular form, termed primitive clay precursors, on the feldspar surface. These precursors, formed by weathering, grow on the surface of the grain, whereas the nanoscale particles of pseudotachylyte identified in the present study are scattered randomly among the submicron fragments, not on the grain surface (Figs. 4c, 6a, 8a).

In the present study, TEM observations reveal that the nanoscale particles of pseudotachylyte are 20–30 nm in size and have irregular shapes (Fig. 7a). These particles have biotite compositions (see below; Figs. 8b, 11b), clearly indicating that they are not amorphous silica, allophone, imogolite, or ferrihydrite. Moreover, this pseudotachylyte is negligibly affected by hydrothermal alteration and chemical weathering following fault movement, as discussed above. For these reasons, we suggest that the nanoscale amorphous material in the pseudotachylyte formed by comminution rather than hydrothermal alteration and chemical weathering following fault movement.

The SiO_2 content of the Iida pseudotachylyte, as determined by XRF-EDS, indicates a granitic source rock. Lin (1996) also reported similar average bulk chemical compositions for the Iida pseudotachylyte and host rock, as determined using XRF, and suggested that the pseudotachylyte formed from the granitic host rock, which consists primarily of quartz, feldspar, and biotite (Lin, 1997a). In the present study, XRF-EDS analyses revealed slightly different bulk chemical compositions for the pseudotachylyte and host rock, as described above. Given that the pseudotachylyte veins cut deformed biotite in the host rock (Fig. 3c, d), and that biotite is rich in TiO_2, Fe_2O_3, and MgO, we assume that the discrepancy in bulk chemical composition reflects differences in the

biotite contents of the pseudotachylyte and host rock. XRF-EDS analyses also reveal that the pseudotachylyte is likely to contain more biotite than the host rock, and that the compositions of the elongated fragments and nanoscale tabular particles in the pseudotachylyte matrix, which consist of Mg, Al, Si, K, Ti, and Fe, are biotite compositions (Figs. 8a, b, 11).

SEM-EDS analyses reveal that the pseudotachylyte matrix consists primarily of biotite composition (Fig. 10); however, peaks for mica clay minerals were not detected in the XRD patterns of the analyzed pseudotachylyte (Fig. 8). Lin (1996, 1997b) also reported the absence of XRD peaks for mica clay minerals that formed by hydrothermal alteration; however, the Iida pseudotachylyte is only weakly affected by hydrothermal alteration after fault movement (see above). We suggest that the absence of peaks for mica clay minerals in the Iida pseudotachylyte probably reflects the amorphization of biotite during the comminution process.

The amorphous material reported by Yund *et al.* (1990) from granite gouges produced by rotary shear sliding experiments has a feldspathic composition; however, the granite sample used in these earlier experiments was homogeneous and mainly composed of feldspar (67%), with just 5% biotite. In contrast, the host cataclasite of the Iida pseudotachylyte contains a foliation defined by the preferred orientation of biotite. The fact that the pseudotachylyte veins cut across deformed biotite in the host rock suggests that the pseudotachylyte was probably generated in the biotite-rich layers within the foliation. Shimada *et al.* (2004) and Toyoshima *et al.* (2004) reported that pseudotachylytes from the Hidaka metamorphic belt are concentrated along thin mylonitic foliation planes defined by a strong preferred orientation of micas. Accordingly, we propose that the difference between the findings of Yund *et al.* (1990)

and the present study, in terms of the composition of amorphous material, reflects differences in the compositions of the host rocks.

XRD peaks for mica clay minerals were only detected in the host rock, not in the pseudotachylyte (Fig. 8). In addition, biotite fragments picked from the host rock are in single-crystal form (Fig. 7c), clearly suggesting that the amorphization of the biotite occurred by comminution during the formation of pseudotachylyte. Grain-size reduction by comminution is commonly attributed to wear and the attrition of quasi-static cumulative slip on the sliding surface induced by progressive shear stress (e.g., Marone and Scholz, 1989). Other recent studies have reported comminution processes attributed to dynamic rock pulverization induced by unloading–loading cycles of normal stress during the propagation of earthquake rupture (e.g., Brune, 2001; Wilson et al., 2005; Reches and Dewers, 2005). Based on the observation of a random fabric and the absence of localized slip zones, Lin et al. (1994) proposed that the Iida pseudotachylyte formed during seismic fault motion. Accordingly, we interpret that the amorphization of biotite in the Iida pseudotachylyte was induced by progressive shear stress during quasi-static slip and normal stress during dynamic rock pulverization on the sliding surface of the fault.

On the basis of rotary shear sliding experiments, Goldsby and Tullis (2002) and Di Toro et al. (2004) suggested that amorphization and the formation of gel via shearing and comminution under wet conditions is one of the weakening mechanisms of faults during seismic slip. It is therefore possible that the amorphous material in the Iida pseudotachylyte induced slip weakening during seismic slip; however, further work is required to reveal whether the amorphous material with biotite content is capable of forming a gel.

Recent studies of experimental and natural pseudotachylytes reveal that comminution is an essential precursor to frictional melting (e.g., Spray, 1995; Curewitz and Karson, 1999; Otsuki et al., 2003). During the comminution process, the activity of fragments within the pseudotachylyte increases with increasing specific surface energy and internal energy of the fragments due to grain-size reduction and the formation of lattice defects, lattice distortion, and an amorphous phase within the fragments (e.g., Kubo, 1963; Kubo and Miyazaki, 1968; Lin and Nadiv, 1979). We assume that the nanoscale to submicron fragments in the Iida pseudotachylyte are likely to have been activated, as the fragments were comminuted to the nanoscale and underwent amorphization and lattice distortion.

Many studies on the grinding of quartz, clay minerals, calcite, and metal oxides such as Fe_2O_3, TiO_2, and ZnO have reported that an increase in the activity of fragments arising from lattice distortion and amorphization during comminution acts to change their physical and chemical properties, including a lowering of the temperature of transformation, the dehydration of structural water, and increased solubility in water (e.g., Gregg et al., 1954; Burns and Bredig, 1956; Kubo, 1963; Kubo et al., 1963; Senna et al., 1971; Lin and Somasundaran, 1972). However, the changes that occur in biotite during the comminution process remain poorly understood. Unlike crystalline materials, amorphous materials do not generally have a specific melting temperature; instead, such materials show a gradual change in melting over a wide range of temperature (e.g., Gwinn et al., 1988). To clarify the frictional melting process of pseudotachylyte, further work is required to gain an understanding of the changes in physical and chemical properties that take place during the comminution process in biotite and the melting behavior of amorphous material formed by comminution.

References

Allen, A. R., 1979, Mechanism of frictional fusion in fault zones. *Journal of Structural Geology*, **1**, 231–243.

Berlenbach, J.W. and Roering, C., 1992, Sheath-fold-like structures in psuedotachylytes. *Journal of Structural Geology*, **14**, 847–856.

Brune, J. N., 2001, Fault normal dynamic loading and unloading: an explanation for "nongouge" rock powder and lack of fault-parallel shear bands along the San Andreas fault. EOS Transactions of American Geophysical Union, 2001 Fall Meeting Abstract, 82, S22B–0655.

Burns, J. H. and Bredig, M. A., 1956. Transformation of calcite to aragonite by grinding. *Journal of Chemical Physics*, **25**, 1281–1282.

Chester, F. M., Evans, J. P. and Biegel, R. L., 1993, Internal structure and weakening mechanisms of the San Andreas Fault. *Journal of Geophysical Research*, **98**, B1, 771–786.

Chester, J. S., Kronenberg, A. K., Chester, F. M. and Gullemette, R. N., 2003, Characterization of natural slip surface relevant to earthquake mechanics. EOS Transactions of American Geophysical Union, 2003 Fall Meeting Abstract, 84, S42C-0185.

Curewitz, D. and Karson, J. A., 1999, Ultracataclasis, sintering, and frictional melting in pseudotachylytes from East Greenland. *Journal of Structural Geology*, **21**, 1693–1713.

De Carli, P. S. and Jamieson, J. C., 1959, Formation of an amorphous form of quartz under shock conditions. *Journal of Chemical Physics*, **31**, 1675–1676.

Dell' Angelo, L. N., Tullis, J. and Yund, R.A., 1987, Transition from dislocation creep to melt-enhanced diffusion creep in fine-grained granitic aggregate. *Tectonophysics*, **139**, 325–332.

Dengler, L., 1976, Microcracks in Crystalline Rocks. In: Wenk, H. R. (Ed.), Electron Microscopy in Mineralogy. Springer-Verlag, Berlin, New York, pp. 550–556.

Di Toro, G., Goldsby, D. L. and Tullis, T. E., 2004, Friction falls towards zero in quartz rock as slip velocity approaches seismic rates. *Nature*, **427**, 436–439.

Fairbairn, H. W. and Robson, G.. M., 1942, Breccia at Sudbury, Ontario. *Journal of Geology*, **50**, 1–33.

Goldsby, D. L. and Tullis, T. E., 2002, Low frictional strength of quartz rocks at subseismic slip rates. *Geophysical Research Letters*, **29**, doi: 10.1029/2002GL015240.

Gregg, S. J., Parker, T. W. and Stephens, J. M., 1954, The grinding of kaolinite. II. A more detailed study. *Journal of applied chemistry*, **4**, 666–674.

Gwinn, R. P., Norton, P. B. and Goetz, P. W., 1988, The New Encyclopaedia Britannica; vol. 7, 15th ed, Encyclopaedia Britannica, Chicago.

Henley, R. W. and Ellis, A. J., 1983, Geothermal systems ansient and modern: A geochemical review. *Earth-Science Reviews*, **19**, 1–50.

Kanaori, Y., Miyakoshi, K., Kakuta, T. and Satake, Y., 1980, Dating fault activity by surface textures of quartz grains from fault gouges. *Engineering Geology*, **16**, 243–262.

Kanaori, Y., Miyakoshi, K., Kakuta, T. and Satake, Y., 1982, Dating fault activity by surface textures of quartz grains from fault gouges (Part I). *Journal of Japan Society of Engineering Geology*, **23**, 18–32 (in Japanese, with English abstract).

Kanaori, Y., 1983, Fracturing mode analysis and relative age dating of faults by surface textures of quartz grains from fault gouges. *Engineering Geology*, **19**, 261–281.

Kano, K., Lin, A., Fukui, A. and Tanaka, H., 2004, Pseudotachylytes of crushing origin from the Shimotsuburai Fault of the Itoigawa-Shizuoka Tectonic Line active fault system, Central Japan. *Journal of Geological Society of Japan*, **110**, 779–790 (in Japanese with English abstract).

Kennedy, L. A. and Spray, J. G., 1992, Frictional melting of sedimentary rock during high-speed diamond drilling: an analytical SEM and TEM investigation. *Tectonophysics*, **204**, 323–337.

Kiefer, S. W., Phakey, P. P. and Christie, J. M., 1976, Shock processes in porous quartzite: transmission electron microscope observation and theory. *Contributions to Mineralogy and Petrology*, **59**, 41–93.

Krinsley, D. H. and Doornkamp, J. C., 1973, Atlas of quartz sand surface textures. Cambridge University Press, London.

Krumbein, W. C., 1941, Mesurement and geologic significance of shape and roundness of sedimentary particles. *Journal of Sedimentary Petrology*, **11**, 64–72.

Kubo, T., 1963, Reactivity of finely pulverized substances. *Chemistry and Chemical Industry*, **16**, 901–915 (in Japanese).

Kubo, T., Kato, M., Mitarai, M., Takahashi, J. and Ohkura, K., 1963, Structural change of TiO2 and ZnO by means of mechanical grinding. *Kogyo Kagaku Zasshi*, **66**, 318–321 (in Japanese).

Kubo, T. and Miyazaki, T., 1968, Mechanochemistry of inorganic substance. J*ournal of Chemical Society of Japan*, **71**, 1301–1309 (in Japanese).

Laws, W. D. and Page, J. B., 1946, Changes produced in kaolinite by dry grinding. *Soil Science*, **62**, 319–336.

Leeder, M. R., 1982, Sedimentology process and product. George Allen & Unwin Ltd, London.

Lin, A., 1994, Glassy pseudotachylyte veins from the Fuyun Fault zone, Northwest China. *Journal of Structural Geology*, **16**, 71–83.

Lin, A., Matsuda, T. and Shimamoto, T., 1994, Pseudotachylyte from the Iida-Matsukawa Fault, Nagano Prefecture: Pseudotachylyte of crush origin? *Journal of the Tectonic Research Group of Japan*, **39**, 51–64 (in Japanese with English abstract).

Lin, A., 1996, Injection veins of crushing-originated pseudotachylyte and fault gouge formd during seismic faulting. *Engineering Geology*, **43**, 213–224.

Lin, A., 1997a, Ductile deformation of biotite in foliated cataclasite, Iida-Matsukawa Fault, Central Japan. *Journal of Asian Earth Sciences*, **15**, 407–411.

Lin, A., 1997b, Fuluidization and rapid injection of crushed fine-grained materials in fault zones during episodes of seismic faulting. In: Zheng et al (Eds.), Proceedings of the 30th International Geological Congress, **14**. VSP, pp. 27–40.

Lin, A., 1999, Roundness of clasts in pseudotachylytes and cataclastic rocks as an indicator of frictional melting. *Journal of Structural Geology*, **21**, 473–478.

Lin, A., Matsushima, N. and Maruyama, T, 2000, Late Quaternary acivity of the Iida-Matsukawa fault in the southern Ina valley, Japan. *Journal of Geological Society of Japan*, **106**, 413–425 (in Japanese, with English abstract).

Lin, A., Shimamoto, T., Maruyama, T., Shigetomi, M., Miyata, T., Takemura, K., Tanaka, H., Uda, S. and Murata, A., 2001, Comparative study of cataclastic rocks from a drill core and outcrops of the Nojima Fault zone on Awaji Island, Japan. *The Island Arc*, **10**, 368–380.

Lin, I. J. and Somasundaran, P., 1972, Alterlations in properties of samples during their preparation by grinding. *Powder Technology*, **6**, 171–179.

Lin, I. J., Nadiv, S. and Grodzian, D. J. M., 1975, Changes in the state of solids and mechano-chemical reactions in prolonged comminution·processes. *Minerals Science and Engineering*, **7**, 313–336.

Lin, I. J. and Nadiv, S., 1979, Review of the phase transformation and synthesis of inorganic solids obtained by mechanical treatment (Mechanochemical reactions). *Material Science and Engineering*, **39**, 193–209.

Mackenzie, R. C. and Milne, A. A., 1953a, The effect of grinding on micas. *Clay Minerals Bulletin*, **2**, 57–62.

Mackenzie, R. C. and Milne, A. A., 1953b, The effect of grinding on micas. I. Muscovite. *Mineralogical magazine*, **30**, 178–185.

Maddock, R. H., 1983, Melt origin of fault-generated pseudotachylytes demonstrated by textures. *Geology*, **11**, 105–108.

Maddock. R. H., 1986, Partial melting of lithic porphyroclasts in fault-generated pseudotachylytes. *Neues Jahrbuch fuer Mineralogie. Abhandlungen*, **155**, 1–14.

Maddock. R. H., Grocott, J. and Van Nes, M., 1987, Vesicles, amygdales and similar structures in fault-generated pseudotachylytes. *Lithos*, **20**, 419–432.

Magloughlin J. F., 1989, The nature and significance of pseudotachylite from the Nason terrane, North Cascade Mountains, Washington. *Journal of Structural Geology*, **11**, 907–917.

Magloughlin. J. F., 1992, Microstructural and chemical changes associated with cataclasis and frictonal melting at shallow crust level: The cataclasite-pseudotachylyte connection. *Tectonophysics*, **204**, 243–260.

Magloughlin, J. F., 2005, Immiscible sulfide droplets in pseudotachylyte: Evidence for high temperature (>1200 C^0) melts. *Tectonophysics*, **402**, 81–91.

Marone, C. and Scholz, C. H., 1989, Particle-size distribution and microstructures within simulated fault gouge. *Journal of Structural Geology*, **11**, 799–814.

Marumo, K. 1995, Fundamental features of amorphous materials in the Earth surface. *Chishitusu News*, **496**, 11–18 (in Japanese).

Oinuma, K. and Kodama, H., 1967, Use of infrared absorption spectra for identification of clay minerals in sediments, *Journal of the Toyo University. General education. Natural science*, **7**, 1–23.

Otsuki, K., Monzawa, N. and Nagase, T., 2003, Fluidization and melting of fault gouge during seismic slip: Identification in the Nojima Fault zone and implications for focal earthquake mechanisms. *Journal of Geophysical Research*, **108**, B4, 2192, doi:10. 1029/2001JB001711.

Perez-Rodriguez, J. L., Madrid Sanchez Del Villar, L. and Sanchez-Soto, P. J., 1988, Effects of dry gringing on pyrophyllite. *Clay Minerals*, **23**, 399–410.

Philpotts, A. R., 1964, Origin of pseudotachylytes. *American Journal of Science*, **262**, 1008–1035.

Ray, R. C., 1923, The effect of long grinding on quartz. *Proceedings of Royal Society A* , **102**, 640–642.

Reches, Z. and Dewers, T. A., 2005, Gouge formation by dynamic pulverization during earthquake rupture. *Earth and Planetary Science Letters*, **235**, 361–374.

Reynolds, D. L., 1954, Fluidization as a geological process, and its bearing on the problem of intrusive granites. *American Journal of Science*, **252**, 577–613.

Sakabe, H., Kohyama, N., Shinohara, Y. and Koshi, K., 1998, Solubility in physiological solution and high-resolution TEM observation of amorphous surface layer of ground quartz particles. In: Chiyotani, K., Hosoda, Y. and Aizawa, Y (Eds.), Advances in the Prevention of Occupational Respiratory Diseases: proceedings of the 9th International Conference on Occupational Respiratory Diseases, Kyoto, pp. 943–947.

Senna, M., Tojo, S. and Kuno, H., 1971, Polymorphic transformation of γ-Fe2O3 by isothermal ball-milling and vacuum hot-pressing. *Nippon Kagaku Zasshi*, **92**, 780–784 (in Japanese).

Shimada, K., Tanaka, H., Toyoshima, T., Obata, T. and Niizato, T, 2004, Occurrence of mylonite zones and pseudotachylyte veins around the base of the upper crust: An example from the southern Hidaka metamorphic belt, Samani area, Hokkaido, Japan. *Earth Planet Space*, **56**, 1217–1223.

Shimazu, M., 1962, Structural change of silica minerals by dry mechanical grinding (I), quartz. *Journal of Mineralogical Society of Japan*, **5**, 291–310 (in Japanese).

Sibson, R. H., 1975, Generation of pseudotachylyte by ancient seismic faulting. *Geophysical Jornal of Royal Astronomical Society*, **43**, 775–79.

Shigetomi, M. and Lin, A., 1999, Seismic events inferred from the layering structures of fault gouge zone and pseudotachylytes in the Nojima Fault zone, Japan. *Journal of Tectonic Research Group of Japan*, **43**, 33–42 (in Japanese with English abstract).

Spray, J.G., 1989, Slickenside formation by surface melting during the mechanical excavation of rock. *Journal of Structural Geology*, **11**, 895–905.

Spray, J.G., 1995, Psedotachylyte controversy: Fact or friction? *Geology*, **23**, 1119–1122.

Takahashi, H., 1959, Effects of dry grinding on kaolin minerals. I. kaolinite. *Bulletin of Chemical Society of Japan*, **32**, 235–245.

Tazaki, K., 1986. Observation of primitive clay precursors during microcline weathering. *Contributions to Mineralogy and Petrology*, **92**, 86–88.

Toyoshima, T., Obata, T., Niizato, T., Shimada, K., Komatsu, M., Wada, Y. and Koyasu, T., 2004, Pseudotachylytes, related fault rocks, asperities, and crustal structures in the Hidaka metamorphic belt, Hokkaido, northern Japan. *Earth Planets Space*, **56**, 1209–1215.

Yoder, H.S. and Eugster, H. P., 1955, Synthetic and natural muscovites. *Geochimica et Cosmochimica Acta*, **8**, 225–280.

Yund, R. A., Blanpied, M. L., Tullis, T. E. and Weeks, J. D., 1990, Amorphous material in high strain experimental fault gouges. *Journal of Geophysical Research*, **95**, 15589–15602.

Wenk, H. R., 1978, Are psudotacylytes products of fracture or fusion? *Geology*, **6**, 507–511.

Willson, B., Dewers, T., Reches, Z. and Brune, J. N., 2005, Particle size and energetics of gouge from earthquake rupture zones. *Nature*, **434**, 749–752.

Part 2 Differentiation and origin of the amorphous materials in pseudotachylyte revealed by transmission electron microscopic observations

1. Introduction

Pseudotachylyte is a dense, aphanitic, veined fault rock thought to be formed by comminution or frictional melting of rocks resulting from fault movement (Philpotts, 1964; Sibson, 1975; Wenk, 1978; Takagi, 1991; Lin, 2008). The first report of pseudotachylyte in Japan described its discovery in a shear zone in the main belt of the Hidaka Metamorphic Belt, Hokkaido (Toyoshima, 1990). After this report, pseudotachylyte was found in shear zones in granitic and metamorphic rock masses in various parts of Japan; for example, from the Iida–Matsukawa Fault (Lin *et al.*, 1994; Lin, 1996); the Hatagawa Fault Zone (Kubo and Takagi, 1997; Takagi *et al.*, 2000), Yawatahama Oshima (Komatsu 1997), the Nojima Fault (Shigetomi and Hayashi, 1999; Fukuchi, 2003; Otsuki *et al.*, 2003), the Osumi Granodiorite Mass (Fabbri *et al.*, 2000), the Median Tectonic Line (Shimada *et al.*, 2001), the Asuke Shear Zone (Takagi and Sakamaki, 2003; Sakamaki *et al.*, 2006), and the Shimotsuburai fault of the Itoigawa–Shizuoka Tectonic Line active fault system (Kano *et al.*, 2004). Recently it was also found in faults developed in accretionary prisms (Ikezawa *et al*, 2003; Mukoyoshi *et al.*, 2006; Okamoto *et al.*, 2006). Some reports describe a type of pseudotachylyte of crush-origin with no melt-quenched texture (Lin *et al.*, 1994; Lin, 1996; and Kano *et al.*, 2004). However, most pseudotachylytes found so far both in Japan and overseas have a melt-quenched texture characterized by a spherulites, microlites, amorphous materials, amygdules, vesicles, embayment texture, or sulfide blebs (Philpotts, 1964; Sibson, 1975; Allen, 1979; Maddock, 1983, 1986; Maddock *et*

al., 1987; Magloughlin, 1989, 1992, 2005; Lin, 1994).

In the melt-quenched texture, amorphous materials are often found by X-ray diffraction or electron diffraction (e.g., Allen, 1979; Magloughlin, 1992; Lin, 1994; Morishita, 1998). Since X-ray diffractometry of the pseudotachylytes in the Iida–Matsukawa and Shimotsuburai faults did not show amorphous materials, those pseudotachylytes were advocated as having a crush-origin (Lin *et al.*, 1994; Kano *et al.*, 2004). However, we identified amorphous materials in the Iida–Matsukawa Fault in nano-size comminuted particles by electron diffraction, and reported that the materials were produced in the comminution process during a fault movement (Ozawa and Takizawa, 2007). We earlier reported the presence of amorphous materials in a fault gouge at Arakurakita in the Itoigawa–Shizuoka Tectonic Line observed by electron diffraction and attributed them to comminution by fault movement (Takizawa and Ozawa, 2006). Experiments also confirmed that amorphous materials were formed from wear or shear of crystalline materials such as quartz, biotite, clay minerals, and granite (e.g., Yoder and Eugster, 1955; Takahashi, 1959; Shimazu, 1962; Yund *et al.*, 1990; Ozawa *et al.*, 2006). Those reports suggest that the presence of amorphous materials alone does not unambiguously constitute evidence of melt-quenching. A lot of research that identified amorphous materials by electron diffraction used samples prepared by ion milling. Although this method is suitable for texture observation, it is highly likely to make amorphous materials during sample preparation, making it difficult to differentiate amorphous materials created during ion milling from naturally formed ones.

We used a transmission electron microscope (TEM) to observe the pseudotachylyte in the Hatagawa Fault Zone, Fukushima Prefecture. This pseudotachylyte contains

spherulites, which are apparent melt-quenched textures. Samples used for observation of microstructures were prepared by ion milling. The presence of amorphous materials was examined in samples prepared by a crushing method, which is less likely to turn samples into an amorphous state during preparation. In the matrix, we identified amorphous materials that show a uniform contrast in bright-field images. The texture is different in microstructure from the amorphous material contained in the pseudotachylyte of crush-origin in the Iida–Matsukawa Fault, Nagano Prefecture. As earlier mentioned, many pseudotachylytes were reported to contain amorphous materials, which are presumably attributable to the melt-quenching process (e.g., Allen, 1979; Magloughlin, 1992; Lin, 1994; Morishita, 1998). But considering that amorphous materials generated from comminution have been found in both comminution experiments and natural pseudotachylytes (e.g., Yoder and Eugster, 1955; Takahashi, 1959; Shimazu, 1962; Yund et al., 1990; Ozawa et al., 2006; Ozawa and Takizawa, 2007), the amorphous materials in pseudotachylytes could have been produced by either melt-quenching or comminution. To corroborate this assumption, we conducted melting and low-speed shear experiments with the host rock of pseudotachylytes and conducted TEM observations of the texture of the amorphous materials formed from each process. Here we discuss the origin of the amorphous materials in the pseudotachylyte in the Hatagawa Fault Zone, recognizing the characteristics of the amorphous materials formed in each experiment, and show the differences between these amorphous materials and those found in the pseudotachylyte of crush-origin in the Iida–Matsukawa Fault. We propose the technique as a way to differentiate the origin of pseudotachylyte using the amorphous materials in the pseudotachylyte.

2. The geology of the Hatagawa Fault Zone

Located at the eastern edge of the Abukuma Mountain Range in Fukushima Prefecture, the Hatagawa Fault Zone has three faults developed in the north-northwest to south-southeast strike, parallel with the Futaba Fault Zone, the center of which is considered to be a tectonic line that divides the Nanbu Kitakami and Abukuma zones (Sendo, 1958; Kubo and Yamamoto, 1990; and Kubo *et al.*, 1990) (Fig. 2-1a). The total displacement of the fracture zone is estimated to be 60 km and left-lateral, judging from the distribution of pre-Cretaceous sedimentary and metamorphic rocks sandwiching the fracture zone, which consists of multiple faults (Otsuki and Nagahiro, 1992).

The Hatagawa Fault Zone occurs in the granite mass of the Lower Cretaceous and is composed of three structural elements: the cataclasite zone with the granite mass as the source rock, the left-lateral mylonite zone, and small-scale shear zones (Tomita *et al.*, 2002) (Fig. 2-1b). Spreading over 50 to 100 m in width, the cataclasite zone runs continuously for over 40 km. Since the alteration minerals in the cataclasite are mainly chlorite, epidote, and calcite, with no clay minerals (montmorillonite, for example), the cataclasite zone is estimated to have been active in an environment of $\geq$220 °C (Tomita *et al.*, 2002). Considering that it is severed by an undeformed granodiorite porphyry dike that shows a hornblende K-Ar age of 98.1 ± 2.5 Ma, the zone is believed to have ended its major activation before that period (Tomita *et al.*, 2002). An overprinting relation among pseudotachylytes is found at one of the outcrops in the cataclasite zone (Shigematsu *et al.*, 2003). The left-lateral mylonite has a maximum width of 1 km, and its distribution is not uniform (Fig. 2-1b). For example, in the area south of the Uketo River, where the outcrop that produced the pseudotachylytes reported here is located, the granites east of the cataclasite zone widely underwent left-lateral plastic deformation,

30

while the granites west of it are almost undeformed. The microstructure of the left-lateral mylonite is divided into Microstructures A and B depending on the characteristics of quartz and feldspar, and these two structures are taken to reflect the differences in deformation conditions (Shigematsu and Yamagishi, 2002; Shigematsu *et al.*, 2003). The deformation temperatures of Microstructures A and B mylonites, measured with a two-feldspar thermometer, are 300 to 360 °C and 340 to 480 °C, respectively, which are thought to indicate the temperatures during deformation (Shigematsu and Yamagishi, 2002; Shigematsu *et al.*, 2003). The Microstructure A mylonite, created by deformation in a relatively cool environment, has a limited distribution, seen only in an area of approximately 6 km in length along a fracture zone near the Uketo River, including the research site (Shigematsu *et al.*, 2003). That area is characterized by uneven plastic deformation, changing every few meters from minor to extreme. Mylonites under the largest deformation turned into ultramylonites, in which repeated plastic deformations and fractures are observed. This suggests that the low-temperature deformation zone near the Uketo River was deformed in the brittle-plastic transition zone.

3. Occurrence of pseudotachylyte in the outcrop

The pseudotachylyte reported here is exposed on an outcrop near the riverbed on the left bank of a channel downstream of a sediment control dam along a tributary of the Uketo River, located south of a quarry in Hirusone, Namie town, Fukushima Prefecture. The outcrop is located in a left-lateral mylonite zone approximately 500 m east of the cataclasite zone that spreads for some 40 km along the Hatagawa Fault Zone, in an area identified as a former epicentral zone (Shigematsu *et al.* 2003) (Fig. 2-1b).

Mylonites derived mainly from granodiorites are distributed around the outcrop, with almost vertical foliation and a strike in the north to south or in the north-northeast to south-southwest direction. In the mylonites, a cataclasite zone approximately 1 m wide is developed, in which pseudotachylytes are found. The major fault vein of the pseudotachylyte is almost parallel with the fracture zone, that is, in a north–south strike, and has an apporoximately 80° east dip. The other boundary of the granodiorite mylonites is cut by a mylonited quartz porphyry dike that intrudes in the north–south direction (Fig. 2-2a, b).

The pseudotachylyte at the outcrop is dark green to gray green and has a veined structure up to 1 cm in width. The boundary between the pseudotachylyte and the host rock is very clear (Figs. 2-2c, 2-3a, 2-3b). The fault vein continues for 10 m, with branches partly developed (Fig. 2-3c), and is fractured and transformed into cataclasite at its end (Fig. 2-3d). Injection veins that laterally inject from the fault vein are apparent at a few locations (Fig. 2-3e).

4.Analytical methods

We observed the microstructure in the matrix of the pseudotachylyte and identified the amorphous materials by TEM (JEOL Ltd., JEM-100CX; acceleration voltage, 100 kV). Samples were prepared by ion milling for observation of the microstructure inside the matrix of the pseudotachylyte, and by crushing for confirmation of amorphous materials in the pseudotachylyte. The specimens prepared by ion milling were samples removed in flakes without the use of resins from same rock piece examined through a polarization microscope, and were further thinned by irradiation with an argon ion beam in a vacuum. The specimens prepared by crushing were lightly smashed in an agate

mortar with distilled water and dispersed by ultrasound into a suspension. A few drops of the suspension were put on a microgrid and dried. All samples were carbon-coated before observation. To avoid making the samples amorphous by the electron beam during observation, we took selected-area electron diffraction images immediately after irradiation of the electron beam.

5. Microstructure of pseudotachylyte

When observed through a polarization microscope, the pseudotachylyte is composed mainly of a light-brown aphanitic matrix and is almost devoid of fragments. The fault vein of this pseudotachylyte cuts the cataclasite with a clear boundary (Fig. 2-4a). Spherulites, approximately 50 to 200 μm in diameter, are apparent in part of the matrix of the fault vein (Fig. 2-4b). Spherulites are formed by rapid cooling of the melt or by crystallization of glass and are often found in igneous rocks (e.g., Lofgren, 1971a, b; Holness, 2002). They are also reported to have been found in pseudotachylytes, and are taken to suggest a melting origin (Maddock, 1986; Magloughlin, 1989). We found a recrystallized texture in the spherulites in the pseudotachylyte (Fig. 2-4c, d). Lofgren (1971a) experimented with the devitrification of obsidian and reported the formation of a similar texture. Therefore, we took TEM samples prepared by ion milling from the matrix of the pseudotachylyte where polarization microscopy showed no clear spherulites.

TEM of the microstructure inside the matrix of the pseudotachylyte revealed amorphous materials, which show a very bright and uniform contrast in the bright-field image and no clear grain boundary inside (Fig. 2-5a). In the bright-field image, when samples have almost the same thickness, amorphous samples look brighter than crystal

samples because the amorphous materials don't cause diffraction and therefore have a greater intensity of transmitted waves than crystals. Conversely, the particles that look darker near the center in the lower part are crystals, and the boundary between them and the amorphous materials is very clear. Amorphous materials penetrating among crystal particles are also apparent (Fig. 2-5a). Amorphous materials that show a very bright and uniform contrast were also found in the samples prepared by crushing (Fig. 2-5b).

6. Discussion

TEM observations revealed amorphous materials in the matrix of the pseudotachylyte produced in the Hatagawa Fault Zone. Since similar amorphous materials were found in samples prepared by ion milling and by comminution, we conclude that they are not formed during ion milling but are originally contained in the samples.

Note that the term "glass" is used to indicate an amorphous material formed by the melt-quenching process (Doremus, 1973; Sakuhana, 1997), and that it is not appropriate to call an amorphous material made from comminution "glass". To avoid confusion, we refrain from using the term.

6.1. Amorphous materials produced by melting experiment

We conducted a melting experiment with the cataclasite, the host rock of pseudotachylyte found in the Hatagawa Fault Zone. Cataclasite lumps were lightly hammered down to powder. The powder was put on sliced molybdenum plates, which were put between the electrodes of a vacuum deposition device. Electricity was applied to the molybdenum plates in a vacuum of ≤ 10–5 mm Hg, and the heat generated melted

the samples. The molten material was crushed and observed by TEM. Amorphous materials that showed a uniform contrast were produced (Fig. 2-5c).

6.2. Amorphous materials formed by low-speed sliding shear

We used granite cataclasite, the host rock of crush-originated pseudotachylyte in the Iida–Matsukawa Fault, for this experiment. Lumps were lightly hammered down, sieved to 125 to 250 μm, and washed to remove finer particles from the surface. The powdery specimens were put between two quartz plates for shear at room temperature in a direct shear test device. A vertical stress of 0.35 MPa was applied to the lower plate to cause a displacement of 1 cm at a constant rate of $5.00 \times 10{-}3$ mm/s. Since the vertical stress is small and the slip rate is slow in this experiment, no frictional heat sufficient to melt the specimens should have been generated. Using Sibson's (1975) equation (8), a maximum shear stress of 0.12 MPa, and a maximum dynamic friction coefficient of 0.34, we calculated the average rising temperature on the slip surface to be no larger than 10^{-3} °C. The shear-pulverized specimens were put in distilled water and dispersed by ultrasonic waves, and the resultant suspension was dropped on a microgrid for TEM. Most of the particles sized from micrometers to ~100 nm were crystalline, and nano-particles of about 50 nm in size became amorphous (Fig. 2-5d).

6.3. Origin of amorphous materials in the pseudotachylyte of the Hatagawa Fault Zone

Yund *et al.* (1990) observed by TEM the gouges formed in a granite and quartzite rotational shear experiment and found amorphous materials that were not melted during gouging but were formed by comminution. Those very fine pulverized particles, <100

nm, coexisted with angular crystal grains of about the same size. The boundary between the amorphous materials and the crystal grains was vague, and characteristically the amorphous materials showed no texture as formed by injection along the crystal grain boundary or cracks. Yund *et al.* pointed out that the amorphous materials formed by melting at high temperatures are characterized by a uniform contrast in the bright-field image and a clear boundary with the crystal grains, and have a different texture from the crush-originated amorphous materials.

The amorphous materials we observed in the pseudotachylyte have a uniform contrast in the bright-field image and show a clear boundary with the crystal grains (Fig. 2-5a). These properties are similar to those of the amorphous materials of melt origin reported by Yund *et al.* (1990). The same texture as formed by injection of the amorphous materials along the particle boundary is also apparent (Fig. 2-5a). The same texture was also found in the pseudotachylyte formed by landslides in Langtang, Nepal, and was proposed as evidence of frictional melting (Masch *et al.*, 1985). Furthermore, our melting experiment results indicate formation of the same amorphous materials that show a uniform contrast as those found in the pseudotachylyte (Fig. 2-5c). These facts suggest that the amorphous materials in the pseudotachylyte of the Hatagawa Fault Zone, Fukushima Prefecture, were produced through the melt-quenching process.

6.4. Comparison with crush-originated amorphous materials

Previously we observed the matrix of the pseudotachylyte in the Iida–Matsukawa Fault by TEM, reported to be crush-originated, and found amorphous materials presumably formed by the comminution of the host rock without undergoing melt-quenching (Ozawa and Takizawa, 2007). Our TEM observation of samples

prepared by ion milling revealed that the matrix of the pseudotachylyte in the Iida–Matsukawa Fault has very small nanoparticles of approximately 20 to 100 nm filling the spaces among crystalline pulverized particles of about 1 μm (Fig. 2-5e). These observations confirm that the amorphous materials in the matrix are concentrated in areas composed of nanoparticles. The TEM samples prepared by crushing also showed amorphous materials present as elongated nanoparticles with an irregular external shape (Fig. 2-5f). Considering that such a texture is also present in the amorphous materials formed in the low-speed sliding shear test and is present as nano-sized particulate matter as earlier mentioned, these characteristics indicate amorphous materials generated by comminution, not melting. The amorphous materials contained in the pseudotachylyte in the Hatagawa Fault Zone and assumed to have been created by melt-quenching are characterized by their indeterminate form, not by a particulate form, and show a uniform contrast in the bright-field image. Those characteristics are very different from those of the crush-originated amorphous materials in the pseudotachylyte in the Iida–Matsukawa Fault as observed by TEM. Those facts and observations show that the origin of amorphous materials found in natural pseudotachylytes may be identified by their structure observed by TEM.

References

Allen, A. R., 1979, Mechanism of frictional fusion in fault zones. *Jour. Struct. Geol.*, **1**, 231–243.

Doremus, R. H., 1973, Glass Science. Wiley, 349p.

Fabbri, O., Lin, A. and Tokushige, H., 2000, Coeval formation of cataclasite and pseudotachylite in a Miocene forearc granodiorite, southern Kyusyu, Japan. *Jour. Struct. Geol.*, **22**, 1015-1025.

Fukuchi, T., 2003, Strong ferromagnetic resonance signal and magnetic susceptibility of the Nojima pseudotachylyte in Japan and their implication for coseismic electromagnetic changes. *Jour. Geophys. Res.*, **108**, B6, ETG, 14-1-14-8.

Holness, M. B., 2002, Spherulitic textures formed during crystallization of partially melted arkose, Rum, Scotland. *Geol. Mag.*, **139**, 651-663.

Ikewsawa, E., Sakaguchi, A. and Kimura, G., 2003, Pseudotachylyte from an ancient accretionary complex: Evidence for melt generation during seismic slip along a master décollement? *Geology*, **31**, 637-640.

Kano, K., Lin, A., Fukui, A. and Tanaka, H., 2004, Pseudotachylytes of crushing origin from the Shimotsuburai fault of the Itoigawa-Shizuoka Tectonic Line active fault system, central Japan. *Journal of Geological Society of Japan*, **110**, 779-790 (in Japanese with English abstract).

Komotsu, M., Miyashita, Y. and Komemushi, S., 1997, Pseudotachylite from the Oshima Island in Yawatahama, western Shikoku, Southwest Japan. *Journal of Geological Society of Japan*, **103**, XXV-XXVI (in Japanese).

38

Kubo, K. and Yamamoto, T., 1990, Cretaceous intrusive rocks of Haramachi district, eastern margin of Abukuma Mountains Petrography and K-Ar age. *Journal of Geological Society of Japan*, **96**, 731-743   (in Japanese with English abstract).

Kubo, K., Yanagisawa, Y., Yoshioka, T., Yamamoto, T. and Takizawa, F., 1990, Geologic. map of the Haramachi and Omika district. Geological Survey of Japan Quadrangle Series Map, scale 1:50000, 155p (in Japanese).

Kubo, K. and Takagi, H., 1997, New finding of pseudotachylyte from the Abukuma Granites on the west of Hatagawa Fracture Zone. *Journal of Geological Society of Japan*, **103**, 798-801(in Japanese).

Lin, A., 1994, Glassy pseudotachylyte veins from the Fuyun fault zone, northwest China. *Jour. Struct. Geol.*, **16**, 71-83.

Lin, A., 1996, Injection veins of crushing-origenated pseudotachylyte and fault gouge formed during seismic faulting. *Engineering Geol.*, **43**, 213-224.

Lin, A., 2008, Fossil Earthquakes: The Formation and Preservation of Pseudotachylytes. Springer, Berlin Heidelberg New York, 348p.

Lin, A., Matsuda, T. and Shimamoto, T., 1994, Pseudotachylyte from the Iida-Matsukawa Fault, Nagano Prefecture: Pseudotachylyte of Crush Origin? *Structural Geology, Journal of the Tectonic Research Group of Japan*, **39**, 51-64 (in Japanese with English abstract).

Lofgren, G., 1971a, Experimentally Produced Devitrification Textures in Natural Rhyolitic Glass. *Geol. Soc. Amer. Bull.*,**82**, 111-124.

Lofgren, G., 1971b, Spherulitic Textures in Glassy and Crystalline Rocks. *Jour. Geophys. Res.*, **76**, 5635-5648.

Maddock, R. H., 1983, Melt origin of fault-generated pseudotachylytes demonstrated by textures. *Geology*, **11**, 105–108.

Maddock. R. H., 1986, Partial melting of lithic porphyroclasts in fault-generated pseudotachylytes. *Neues Jahrb., Mineral. Abh.*, **155**, 1-14.

Maddock. R. H., Grocott, J. and Van Nes, M., 1987, Vesicles, amygdales and similar structures in fault-generated pseudotachylytes. *Lithos*, **20**, 419–432.

Magloughlin J. F., 1989, The nature and significance of pseudotachylite from the Nason terrane, North Cascade Mountains, Washington. *Jour. Struct. Geol.*, **11**, 907-917.

Magloughlin. J. F., 1992, Microstructural and chemical changes associated with cataclasis and frictonal melting at shallow crust level: the cataclasite-pseudotachylyte connection. *Tectonophysics*, **204**, 243-260.

Magloughlin, J. F., 2005, Immiscible sulfide droplets in pseudotachylyte: Evidence for high temperature (>1200 C0) melts. *Tectonophysics*, **402**, 81–91.

Masch, L., Wenk, H. R. and Preuss, E., 1985, Electron microscopy study of hyalomylonites—Evidence for frictional melting in landslide. *Tectonophysics*, **115**, 131-160.

Morisita, T., 1998, Possible pseudotachylyte from the Horoman peridotite complex of the Hidaka belt, Hokkaido, noethern Japan. *Jour. Geol. Soc. Japan*, **104**, 18-23.

Mukoyoshi, H., Sakaguchi, A., Otsuki, K., Hirono, T. and Soh, W., 2006, Co-seismic frictional melting along an out-of-sequence thrust in the Shimanto accretionary complex. Implications on the tsunamigenic potential of splay faults in modern subduction zones. *Earth Planet. Sci. Lett.*, **245**, 330-343.

Okamoto, S., Kimura, G., Takizawa, S. and Yamaguchi, H., 2006, Earthquake fault rock indicating a coupled lubrication mechanism. *eEarth Discuss.*, **1**, 135-149.

Otsuki, K. and Ehiro, M., 1992, Cretaceous left-lateral faulting in Northeast Japan and its bearing on the origin of geologic structure of Japan. *Journal of Geological Society of Japan*, **98**, 1097-1112 (in Japanese with English abstract).

Otsuki, K., Monzawa, N. and Nagase, T., 2003, Fluidization and melting of faule gouge during seismic slip: Identification in the Nokima fault zone and implications for focal earthquake mechanisms. *Jour. Geophys. Res*, **108**, B4, 2192, ESE, 4-1-4-18.

Ozawa, K., Takizawa, S. and Hatta, T., 2006, Noncrystallization of Biotite in Comminution Experiments. The 113th Annual Meeting of the Geological Society of Japan, Abstract, O-97.

Ozawa, K. and Takizawa, S., 2007, Amorphous material formed by the mechanochemical effect in natural pseudotachylyte of crushing origin: A case study of the Iida-Matsukawa Fault, Nagano Prefecture, Central Japan. *Jour. Struct. Geol.*, **29**, 1855-1869.

Philpotts, A. R., 1964, Origin of psudotachylytes. *Amer. Jour.. Sci.*, **262**, 1008-1035.

Sakamaki, H., Shimada, K. and Takagi, H., 2006, Selective generation surface of pseudotachylyte—example from the Asuke Shear Zone, SW Japan—, *Journal of Geological Society of Japan*, **112**, 519-530 (in Japanese with English abstract).

Sakka, S., 1997, Fandation and application of glass science. Uchida rokakuho, 361p.

Sendo, T., 1958, On the granitic rocks of Mt. Otakine and its adjacent districts in the Abukuma massif. *Japan.Sci. Rep. Tohoku u., Third Ser.*, **6**, 57-167.

Shigematsu, N., Fujimoto, K., Ohtani, T., Tanaka, H., Miyashita, Y. and Tomita, T., 2003, Structures of Fault Zones in the Brittle-plastic Transition Zone of the Continental Earth's Crust: A case study of the Hatagawa Fault Zone, *Journal of Geography*, **112**, 2-19 (in Japanese with English abstract).

Shigematsu, N., and Yamagishi, H., 2002, Quartz microstructures and deformation conditions in Hatagawa shaer zone, NE Japan. *Island Arc*, **11**,45-60.

Shigetomi, M. and Lin, A., 1999, Seismic events inferred from the layering structures of fault gouge zone and pseudotachylytes in the Nojima fault zone, Japan. *Structural Geology, Journal of the Tectonic Research Group of Japan*, **43**, 33-42 (in Japanese with English abstract).

Shimada, K., Kobari, Y., Okamoto, T., Takagi, H. and Saka, Y., 2001, Pseudotachylyte veins associated with granitic cataclasite along the Medean Tectonic Line, eastern Kii Peninsula, Southwest Japan. *Jour. Geol. Soc. Japan*, **107**, 117-128.

Shimazu, M., 1962, Structural Change of Silica Minerals by Dry Mechanical Grinding (□), Quartz. *Journal of Mineralogical Society of Japan*, **5**, 291-310.

Sibson, R. H., 1975, Generation of Pseudotachylyte by Ancient Seismic Faulting. *Geophys. J. R. Astr. Soc.*, **43**, 775-794.

Takagi, H., 1991, Pseudotachylyte. Chishitsu News, 437, 15-25 (in Japanese).

Takagi, H., Goto, K., Shigematsu, N., 2000, Ultramylonite bands derived from cataclasite and psudotachylyte in granites, northeast Japan, *Jour. Struct. Geol.*, **22**, 1325-1339.

Takagi, H. and Sakamaki, H., 2003, Fault rocks related to the Asuke shear zone. The 110th Annual Meeting of the Geological Society of Japan, Excursion Guidebook, 1-10 (in Japanese).

Takagi, H., Shimada, K., Saka, Y., Arai, S., Kobari, Y. and Okamoto, T., 2001,Pseudotachylytes in the Ryoke Belt. *Journal of Geological Society of Japan*, **107**,III-IV (in Japanese).

Takahashi, H., 1959. Effects of dry grinding on kaolin minerals. I. kaolinite. *Bull. Chem. Soc. Japan,* **32**, 235–245.

Takizawa, S. and Ozawa, K., 2006, Amorphous Material in Fault Gauges and its Contribution, The 113th Annual Meeting of the Geological Society of Japan, Abstract, O-96 (in Japanese).

Tomita, T., Ohtani, T., Shigematsu, N., Tanaka, H., Fujimoto, K., Kobayashi, Y., Miyashita, Y., and Omura, K., 2002, Development of the Hatagawa Fault Zone clarified by geological and geochronological studies, *Earth Planets Space,* **54**, 1095-1102.

Toyoshima. T., 1990, Pseudotachylite from the Main Zone of the Hidaka metamorphic belt, Hokkaido, northern Japan. *Jour. Metamorphic Geol.,* **8**, 507-523.

Wenk, H. R., 1978, Are psudotacylytes products of fracture or fusion? *Geology,* **6**, 507–511.

Yoder, H.S. and Eugster, H. P., 1955, Synthetic and natural muscovites. *Geochim. Cosmochim. Acta.,* **8**, 225–280.

Yund, R. A., Blanpied, M. L., Tullis, T. E. and Weeks, J. D., 1990, Amorphous material in high strain experimental fault gouges. *Jour. Geophys. Res.,* **95**, 15589–15602.

Part 3   Amorphization of biotite reproduced in the comminution experiment

using a mechanical agate mortar

1. Introduction

Among mechanochemical effects, it is well known that comminution induces phase transformation, such as amorphization and polymorphic transformation in the solid state. It also changes the physical and chemical properties of materials (e.g., Kubo, 1963; Kubo and Miyazaki, 1968; Lin and Nadiv, 1979). The driving forces of phase transformations in the solid state are strain energy, shear energy, thermal energy, sound energy and kinetic energy during comminution processes such as crushing, grinding, pulverizing, and polishing (e.g., Lin et al., 1975; Lin and Nadiv, 1979). There have been numerous reports in the literature of marked amorphization during the crushing or prolonged grinding of materials, such as quartz (e.g., Ray, 1923; De Carli and Jamieson, 1959; Shimazu, 1962; Lin and Somasundaran, 1972; Sakabe et al., 1998), and clay minerals (e.g., Laws and Page, 1946; Mackenzie and Milne, 1953a, b; Yoder and Eugster, 1955; Takahashi, 1959; Perez-Rodriguez et al., 1988), and TiO_2 and ZnO (e.g., Kubo et al., 1963).

Comminution of minerals and gouge or breccia formation is ubiquitous in brittle fault-zones at all scales. Experimental studies of granite and quartzite gouges have revealed that amorphous materials are formed by comminution using by high-pressure rotary-shear apparatus (Yund et al., 1990). Recently, amorphization and silica gel formation via shearing and comminution under wet conditions have been proposed as weakening mechanisms of faults during seismic slip in the rotary-shear experiments (e.g., Goldby and Tullis, 2002; Di Toro et al., 2004). The result of such experimental

studies clearly suggest that the amorphous materials formed by comminution is essential to our understanding of the strength of faults and faulting processes during earthquakes. In addition, some recent studies of the natural fault-related rock have reported that amorphous materials are formed by mechanochemical effects in the comminution process during fault movement. Amorphization of biotite has been found in pseudotachylyte from the Iida–Matsukawa fault in Central Japan (Ozawa and Takizawa, 2007). However, the only experimental information available on the structural changes caused by grinding of biotite is X-ray diffraction data from a preliminary experiment by Mackenzie and Milne (1953) using a mechanical agate mortar. They showed that the X-ray diffraction of biotite after 7 hours of grinding was only slight blurred; amorphization of biotite has therefore not as yet been reported.

In this study, we conducted prolonged comminution experiments on natural biotite. We report the amorphization of biotite, as analyzed by using X-ray diffraction (XRD), scanning electron microscope (SEM), Transmission electron microscope (TEM), and Fourier transform infrared spectrometer (FT-IR).

2. Materials and Methods

The biotite used came from the Silver Crater Mine in Ontario, Canada. Small blocks of biotite were crushed with a microtome and then put through stainless-steel sieves. Powder samples (particle size of 45 to 75 μm) were used as starting materials. A 2.0 g portion of the powder sample was dry-ground in a mechanical agate mortar at room temperature. Samples were withdrawn at the following times: 6, 12, 18, 24, 30, 36, 48, 60, 72, 84, 96, 120, 144, 168, 216, and 312 hours.

XRD patterns were obtained using a RINT RAD-C X-ray diffractometer. The

experimental conditions were as follows: filtered Cu-K$_\alpha$ radiation, X-ray generator at 40 kV, 25 mA, scanning step 0.02°, scanning speed 2°/min, divergence slit 1°, scattering slit 1°, receiving slit 0.15 mm. Each powdered specimen (2 mg) was affixed to an X-ray-non-reflective specimen holder with acetone in the fixed area of a circle 6.5 mm in diameter.

SEM observations were performed with a JEOL JSM-6320F high-resolution scanning electron microscope (HRSEM) with an accelerating voltage of 5 kV. Samples for SEM observations were spread over an aluminium tape subjected to hydrophilic treatment.

TEM analyses were conducted on a JEOL JEM-100CX TEM with an accelerating voltage of 100 kV. Samples for TEM analyses were dispersed on a microgrid without films and coated with carbon.

FT-IR spectra were measured with a HORIBA FREEXACT-II FT-720 Fourier transform infrared (FT-IR) spectrometer in the spectral region between 400 and 4000 cm^{-1}.

3. Results

3.1. X-ray diffraction

The X-ray diffraction patterns are shown in Figure 3-1. The intensity of reflection decreased, and the background intensity increased, with increasing grinding time. The peak at (060) of the starting materials could not be observed, because the background intensity of the starting samples was high. However, the peak was observable after 6 hours of grinding, but by 48 hour, the reflection peak had gradually disappeared with the gradual decrease in intensity. After 120 hours of grinding, all of the reflecting

surfaces of the biotite disappeared and the background intensity had increased.

3.2. SEM observations

The particles in the original biotite samples were elongated (Fig.3-2a).

After 6 hours of grinding, the samples have platy shape (Fig.3-2b). After 12 hours of grinding, the particles had become finer, and formed fine particles with less than 100 nm in diameter (Fig.3-2c). As the grinding continued, these fine particles became more rounded (Figs.3-2c,d), and finally they formed spherical shapes 100 nm in diameter (Fig.3-2f).

3.3. TEM observations

The starting materials were single crystals with platy shapes (Fig. 3-3a). The SAD patterns of the 100 nm sphrical particles resulting from the grinding had an amorphous pattern (Fig. 3-3b).

3.4. FT-IR spectra

The pronounced doublet between wavenumbers 990 cm-1 and 950 cm-1 gradually faded out and changed to a single broad absorption close to 990 cm-1 when the grinding time exceeded 48 hours. The intensities of the absorptions near 715 cm -1 and 680 cm -1 generally decreased as grinding progressed. These absorptions become weak after 48 hours of grinding and broad after 120hours of grinding (Fig. 3-4).

4. Discussion

The results of the XRD analyses showed that the intensity of each reflective

surfaces decreased, and the background intensity increased, during grinding. This indicated that the crystalline biotite gradually changed into amorphous materiales. HRSEM observation reveal that the starting particles were mostly angular. With increasing grinding time, the particles became finely ground and very rounded, ultimately becoming spherical amorphous materials 100 nm in diameter.

The results of the FT-IR spectroscopy analysis also revealed a decrease in crystallinity; this was based on the fact that the absorption broadened as the grinding duration increased. The doublet in the 990 cm^{-1} to 950 cm^{-1} region was indicative of stretching vibration of Si-O-Si, but after 48 hours the sample showed a single broad absorption near 990 cm^{-1}, indicating that disturbance of Si-O-Si bonding had occurred by 48 hours. The absorption near the 715 cm^{-1} and 680 cm^{-1} regions was Si-O-Fe bond absorption; it had broadened by 120 h, indicating that Si-O-Fe bonding disturbance occurred after 120 h of grinding.

The FT-IR spectroscopy results suggested that absorption of Si-O-Si after 48 hours of grinding indicated bonding disturbance, namely disturbance of the systematic structure of the tetrahedral layer. Furthermore, the results of the XRD analysis, which revealed that (060) reflection (an indication of the systematic structure of the octahedral layer) had disappeared, suggested that structural disturbance occurred in the octahedral layer after 48 hours of grinding. In addition, as detected by FT-IR spectroscopy, Si-O-Fe bonding disturbance occurred after 120 hours of grinding and can be considered to represent a disturbance in the systematic sequence of the C-axis orientation of biotite. XRD analysis showed that the most intense diffraction line, at about 26°, had a C-axis-oriented layer structure; the disappearance of the most intense diffraction line in the sample after 120 hours of grinding coincided with the Si-O-Fe bonding disturbance

detected in the FT-IR spectroscopic analysis. From these results, we concluded that the structure of biotite was eventually disturbed three-dimensionally and became amorphized.

References

De Carli, P. S. and Jamieson, J. C., 1959, Formation of an amorphous form of quartz under shock conditions. *Journal of Chemical Physics*, **31**, 1675–1676.

Di Toro, G., Goldsby, D. L. and Tullis, T. E., 2004, Friction falls towards zero in quartz rock as slip velocity approaches seismic rates. *Nature*, **427**, 436–439.

Goldsby, D. L. and Tullis, T. E., 2002, Low frictional strength of quartz rocks at subseismic slip rates. *Geophysical Research Letters*, **29**, doi: 10.1029/2002GL015240.

Kubo, T., 1963, Reactivity of finely pulverized substances. *Chemistry and Chemical Industry*, **16**, 901–915 (in Japanese).

Kubo, T., Kato, M., Mitarai, M., Takahashi, J. and Ohkura, K., 1963, Structural change of TiO2 and ZnO by means of mechanical grinding. *Kogyo Kagaku Zasshi*, **66**, 318–321 (in Japanese).

Kubo, T. and Miyazaki, T., 1968, Mechanochemistry of inorganic substance. *Journal of Chemical Society of Japan*, **71**, 1301–1309 (in Japanese).

Laws, W. D. and Page, J. B., 1946, Changes produced in kaolinite by dry grinding. *Soil Science*, **62**, 319–336.

Lin, I. J. and Somasundaran, P., 1972, Alterlations in properties of samples during their preparation by grinding. *Powder Technology*, **6**, 171–179.

Lin, I. J. and Nadiv, S., 1979, Review of the phase transformation and synthesis of inorganic solids obtained by mechanical treatment (Mechanochemical reactions). *Material Science and Engineering*, **39**, 193–209.

Mackenzie, R. C. and Milne, A. A., 1953a, The effect of grinding on micas.*Clay Minerals Bulletin*, **2**, 57–62.

Mackenzie, R. C. and Milne, A. A., 1953b, The effect of grinding on micas. I. Muscovite. *Mineralogical magazine*, **30**, 178–185.

Ozawa, K. and Takizawa, S., 2007, Amorphous material formed by the mechanochemical effect in natural pseudotachylyte of crushing origin: A case study of the Iida-Matsukawa Fault, Nagano Prefecture, Central Japan. *Jour. Struct. Geol.*, **29**, 1855-1869.

Perez-Rodriguez, J. L., Madrid Sanchez Del Villar, L. and Sanchez-Soto, P. J., 1988, Effects of dry gringing on pyrophyllite. *Clay Minerals*, **23**, 399–410.

Ray, R. C., 1923, The effect of long grinding on quartz. *Proceedings of Royal Society A*, **102**, 640–642.

Sakabe, H., Kohyama, N., Shinohara, Y. and Koshi, K., 1998, Solubility in physiological solution and high-resolution TEM observation of amorphous surface layer of ground quartz particles. In: Chiyotani, K., Hosoda, Y. and Aizawa, Y (Eds.), Advances in the Prevention of Occupational Respiratory Diseases: proceedings of the 9th International Conference on Occupational Respiratory Diseases, Kyoto, pp. 943–947.

Takahashi, H., 1959, Effects of dry grinding on kaolin minerals. I. kaolinite. *Bulletin of Chemical Society of Japan*, **32**, 235–245.

Yoder, H.S. and Eugster, H. P., 1955, Synthetic and natural muscovites. *Geochimica et Cosmochimica Acta*, **8**, 225–280.

Yund, R. A., Blanpied, M. L., Tullis, T. E. and Weeks, J. D., 1990, Amorphous material in high strain experimental fault gouges. *Journal of Geophysical Research*, **95**, 15589–15602.

Part 4 Microstructures of the sliding surfaces formed in crush-origin pseudotachylyte, at high and low slip rates determined by shapes of submicron comminuted particles

1. Introduction

Amorphous particles of approximately 100 nm across were found recently in crush-origin pseudotachylytes of the Iida–Matsukawa fault in Nagano and in the white gouge in the Arakura fault along the Itoigawa–Shizuoka tectonic line in Yamanashi, Japan (Takizawa and Ozawa, 2006; Ozawa and Takizawa, 2007). These particles were presumably produced from rocks comminuted by fault movements. Those in the Iida–Matsukawa fault were elongate, polygonal, or nearly spherical, whereas those in the Arakura fault were nearly spherical. Amorphous particles in fault rocks exhibit a variety of shapes, but the conditions under which the shapes form remain unclear. In the industrial manufacture of fine particles, the shape of comminuted particles depends on the comminution conditions or processes, such as crush strength and speed (e.g., Yokoyama and Kaya, 1977). The heat of friction generated by rotary shear testing machines and its effects and on comminuted particles have been reported (e.g.,Lin and Shimamoto, 1988; Yund et al., 1990; Goldsby and Tullis, 2002; Di toro et al., 2004). However, natural fault movements primarily involve linear slip motions, and most comminution and friction tests do not take into account the conditions in natural movements.

Recent seismic observations identified that faults in brittle regions move not only at high speeds but also at low speeds in an earthquake (e.g., Linde et al., 1996; Yagi and Kikuchi, 2003; Obara and Ito, 2005). This implies that the comminution of rocks caused

by fault movements could occur under various slip rate conditions, which may contribute to the variety of shapes of comminuted particles. Hence, we conducted shear tests at different slip rates in order to elucidate the effects of slip rates on the shape of comminuted particles. We then investigated the conditions of formation of amorphous particles in the pseudotachylytes of the Iida–Matsukawa fault.

2. Sliding shear test:materials and methods

We considered a linear sliding motion at two slip rates: 1 or 5 cm of displacement at <1 cm/s (high-speed condition) and 1 cm of displacement at ~1 cm/30 min (low-speed condition). The Apparatuses used for the direct shear tests are shown in Fig. 4-1. Both tests were conducted at room temperature under dry conditions at a normal stress of 0.35 MPa. We used granular quartz and biotite samples and granite cataclasite samples of the country rock obtained from the pseudotachylytes of the Iida–Matsukawa fault as starting materials (Fig. 4-2).

The biotite used in this study were crushed by a microtome, and then put through stainless steel sieves. The powder sample with particle size of 45 to 75 μm was used as starting material. The quartz used in this study were artificial powder which have 99.9 % purity, and put through stainless steel sieves to 45 to 75 μm which used as starting material. Then, these powder samples were elutriated to remove very fine particles. The granite cataclasite samples were crushed lightly, and then put through stainless steel sieves. The powder sample with particle size of 125 to 250 μm was used as starting material. A thin layer of each powder samples was placed on horizontally precut surface of quatzs cylinder.

We used HRSEM and TEM to observe the shape, grain size, and crystallinity of the

comminuted particles. After the shear tests the comminuted particles were dispersed in distilled water with ultrasonic agitation, then dropped onto a slide glass subjected to hydrophilic treatment. HRSEM observations were made of shape (circularity) and grain size (equivalent circle diameter); These parameters were measured by using Win-Roof software. For TEM observations, the same suspension was dropped onto a microgrid (without films) subjected to hydrophilic treatment. Measurements were performed for comminuted particles less than 10 μm. Samples for HRSEM analyses were covered with platinum, whereas TEM specimens were carbon-coated.

3. Results

3.1. Shapes of submicron particles in sliding shear tests

The shapes of submicron particles differed markedly depending on the slip rate conditions, regardless to the starting materials used. At the high slip rate, most particles were elongated (Fig.4-3). At the low slip rate, in contrast, the particles were polygonal or spherical (Fig.4-4). Figure 4-5 to 4-7 show the relationship between the equivalent circle diameter and the circularity of the comminuted particles less than 10 μm in diameter after the shear slip tests. The circularity varied from 0.00 to 1.00.When the circularity approximated 1.00, the shapes had circular shape. The circularities of the micron-size comminuted particles were distributed in the same regions in the two tests conducted at different sliding speeds, indicating that particle formation exhibited the same trends and that variations in sliding speed caused no differences. However, the submicron particle samples of quartz, biotite, and granite cataclasite differed, especially in the case of particles less than 100 nm. Under high-speed test conditions the circularity of these particles was lower, at no more than 0.8. In contrast, the circularity

of submicron particles increased under low-speed testing, with that of most particles concentrated around the 0.8 to 0.9 region.

3.2. Crystallinity of submicron particles in sliding shear tests

Independent of the slip rate, amorphous particles of ≤ 100 nm were identified when quartz and granite was slid. Although amorphous particles were not observed in biotite, the crystallinity of the particles was considered low, as indicated by electron beam diffraction patterns showing ambiguous diffraction spots or the loss of diffraction spots on certain reflecting surfaces (Figs. 4-3, 4-4).

3.3. Modes of occurrence of submicron comminuted particles in the
Iida-Matsukawa pseudotachylytes

The pseudotachylytes vein of the Iida–Matsukawa fault comprise elongate amorphous particles several hundred nanometers long, and polygonal or nearly spherical particles ~50 nm across. To elucidate the modes of occurrence of these submicron particles, we observed the fracture surface of freeze dried samples by scanning electron microscope. Inside the pseudotachylyte vein, we could see shear planes that were almost parallel with the line of the vein and others that were about 30° oblique to the vein. On the parallel plane, we observed a structure comprising a group of elongate submicron particles with a width of ~10 μm. The long axis of the elongate particles was almost parallel with the line of the pseudotachylyte vein. In addition, on the oblique surface, we observed a structure with polygonal or nearly spherical particles of ~50 nm across scattered among roundish particles of ~500 nm across (Fig. 4-8).

4. Discussion

The results of the sliding shear tests showed that the shapes of the comminuted submicron particles differed markedly depending on the slip rate conditions regardless of starting materials (i.e. quartz, biotite, or granite cataclasite).These result suggest that all type of starting materials—e.g. those with or without cleavages, or rocks consisting of multiple minerals—would exhibit the same trend.

The submicron-sized comminuted particles formed in the sliding shear tests were characterized by a polygonal or nearly spherical shape at a low slip rate. Because similar particles were found on the shear surface that lies oblique to the pseudotachylyte vein in the Iida–Matsukawa fault, this shear surface was therefore likely formed at a slow slip rate. In contrast, elongated amorphous particles were formed at high slip rate; therefore, the shear surface that developed in parallel with the pseudotachylyte vein was presumably formed at a high slip rate, because elongated particles accumulated on the surface. In addition, the parallel and oblique shear surfaces might correspond to the Y- and R-shears, respectively; thus the R- and Y-shears formed in the shear zones might represent the difference in shear slip rates under a unstable yielding(Morgenstern and Tchalenko,1967) during second-order shears (McKinstry, 1953)..

The results of the sliding shear tests at high and low slip rates and the descriptions of pseudotachylytes in the Iida–Matsukawa fault suggest that sliding surfaces formed at high and low slip rates are distinguishable by the shapes of the submicron comminuted particles in fault rocks.

Given the presence of submicron-elongated particles in the matrix of the Iida-Matsukawa pseudotachylte, it was formed by earthquakes. Therefore the submicron amorphous materials in the pseudotachylyte were formed by earthquakes, suggesting

that the dissipative energy responsible for the comminuted particles' crystal structures becoming amorphous may be part of the earthquake dissipative energy. In the commonly employed slip-weakening model, the elastic strain energy released during an earthquake is partitioned between the breakdown energy, the frictional heat, and the energy radiated in the form of seismic waves. The breakdown energy is defined as the excess of energy above some minimum traction level achieved during the slip of the earthquake fault. This energy is equivalent to the fracture energy which is formed the new surface, in previous investigation (e.g., Tinti et al., 2005). However, the surface energy estimated from grain sizes in the gouge from the Chelungpu fault in Taiwan suggests that the contribution of gouge surface energy to the overall breakdown energy is calculated to be 6% (Ma et al., 2006).The results indicate that there is unknown energy in the breakdown energy, which, in this study, is responsible for the crystal structures of the comminuted particles becoming amorphous. We suggest that the new energy found in this study might be part of the breakdown energy.

References

Di Toro, G., Goldsby, D. L. and Tullis, T. E., 2004, Friction falls towards zero in quartz rock as slip velocity approaches seismic rates. *Nature*, **427**, 436–439.

Goldsby, D. L. and Tullis, T. E., 2002, Low frictional strength of quartz rocks at subseismic slip rates. *Geophysical Research Letters*, **29**, doi: 10.1029/2002GL015240.

Lin, A. and Simamoto, T., 1998, Selective melting processes as inferred from experimentally generated pseudotachylytes. *Journal of Asian Erth Sciences*, **16**, 533-545.

Linde, A.T., Gladwin, M. T., Johnston Malcolm J. S., Gwyther, R. L.and Bilham, R. G., 1996, A slow earthquake sequence on the San Andreas fault. *Letter to Nature*, **383**, 65-68.

Ma, K.F., Tanaka, H., Song, S. R.,Wang, C.Y., Hung, J. H.,Tsai, Y.B., Mori, J., Song, Y.F., Yeh, E.C., Soh,W., Sone, H., Kuo,L. W. and Wu, H. Y., 2006,Slip zone and energetics of a large earthquake from the Taiwan Chelungpu-fault Drilling Project. *Nature*, **444**, 473-476.

McKinstry, H.E., 1953, Shears of the second order. *American Jour. Sci*, **25**, 401-414.

Morgenstern, N. R. and Tchalenko, J.S., 1967, Microscopic structures in kaolin subjected to direct shaer. *Geotechnique*, **17**, 309-328.

Obara, K. and Ito, Y., 2005, Verylow frequency earthquakes excited by the 2004 off the Kii peninsulaearthquake: A dynamic deformation process in the largeaccretionary prism. *Earth Planet Spaces*, **57**, 321-326.

Ozawa, K. and Takizawa, S., 2007, Amorphous material formed by the mechanochemical effect in natural pseudotachylyte of crushing origin: A case

study of the Iida-Matsukawa Fault, Nagano Prefecture, Central Japan. *Jour. Struct. Geol.*, **29**, 1855-1869.

Tinti,E., Spudich,P. and Cocco, M., 2005, Earthquake fracture energy inferred from kinematic rupture models on extended faults. *Journal of Geophysical Research*, **110**, B12303, doi:10.1029/2005JB003644.

Yagi, Y., and Kikuchi, M., 2003, Partitioning between Co-seismic Slip and A-seismic Slip. *Journal of Geography*, **112**, 828-836.

Yokoyama, T. and Kaya, N., 1977, Comminution and Mixing of Ceramics; especially on the fine Grinding. *Ceramics*, **12**, 376-391.

Takizawa, S. and Ozawa, K., 2006, Amorphous Material in Fault Gauges and its Contribution, The 113th Annual Meeting of the Geological Society of Japan, Abstract, O-96 (in Japanese).

Yund, R. A., Blanpied, M. L., Tullis, T. E. and Weeks, J. D., 1990, Amorphous material in high strain experimental fault gouges. *Jour. Geophys. Res.*, **95**, 15589–15602.

Conclusions

In this study, natural pseudotachylytes from the Iida–Matsukawa Fault (crush-origin) and the Hatagawa Fault (melt-origin) were described down to the nanometer scale; the amorphous materials in the matrix are particularly noticed. To determine how the amorphous materials formed, we conducted the comminution experiment using a mechanical agate mortar and sliding shear tests under various conditions. The following conclusions have been drawn from this work.

(1) This study is the first to clearly document amorphous material formed by comminution, without the rapid cooling of melt, in natural crush-origin pseudotachylyte. The presence of amorphous material is therefore not always indicative of the rapid cooling of melt in pseudotachylyte. The amorphous material within the matrix of the Iida pseudotachylyte formed due to mechanochemical effects induced by shear stress and normal stress during the comminution process accompanied by fault movement.

(2) Amorphous materials in pseudotachylyte from the Hatagawa Fault Zone (HFZ) in Fukushima Prefecture were analyzed using by transmission electron microscope (TEM). The pseudotachylyte matrix includes amorphous materials which have both irregular shapes and uniform contrast in bright-field image. Their appearances in the TEM images are distinct from those of the amorphous nanopaeticale materials in the crush-origin pseudotachylyte from the Iida-Matsukawa Fault (IMF) in Nagano Prefecture. We also performed both melting experiments of the

host rock of the pseudotachylyte from HFZ and low-speed shear tests of the host rock of the pseudotachylyte from IMF, producing amorphous materials in each experiment. The TEM images also reveal them to have different characteristics. It is suggested that the origin of amorphous materials in pseudotachylyte can be distinguished by their appearances in the TEM images.

(3) In the agate mortar experiment, biotites were found to change from single crystals to amorphous materials by comminution, not melting. The amorphous materials were spherical and 100 nm in diameter.

(4) In the sliding shear tests, the shapes of submicron comminuted particles differed greatly depending on the slip rate conditions. At the high slip rate, most particles were elongated, but at the low slip rate, the particles were polygonal or spherical. These results hold true for all sample types (i.e. quartz, biotite, and granite cataclacite which host rock of the Iida–Matsukawa pseudotachylyte).

(5) Our sliding shear tests at high and low slip rates, along with the descriptions of pseudotachylytes in the Iida–Matsukawa fault, indicated that the elongated amorphous particles in the pseudotachylyte were formed under high-speed conditions during earthquake fault movement. Most of the amorphous materials were formed on the surfaces parallel to the pseudotachylyte vein. In contrast, the polygonal or nearly spherical amorphous particles were formed under low-speed conditions. Most of these particles were scattered in the R-shears of the pseudotachylyte vein.

(6) The submicron amorphous materials in the Iida-Matsukawa pseudotachylyte were formed by earthquakes, suggesting that the new dissipative energy responsible for the comminuted particles' crystal structures becoming amorphous may be part of the earthquake dissipative energy. In particular, we suggest that the new energy found in this study might be part of the breakdown energy.

Acknowledgements

Fig. 1-1 Index map and simplified geological map of the Iida region, southern Nagano Prefecture, Central Japan (modified from Lin, 1996).
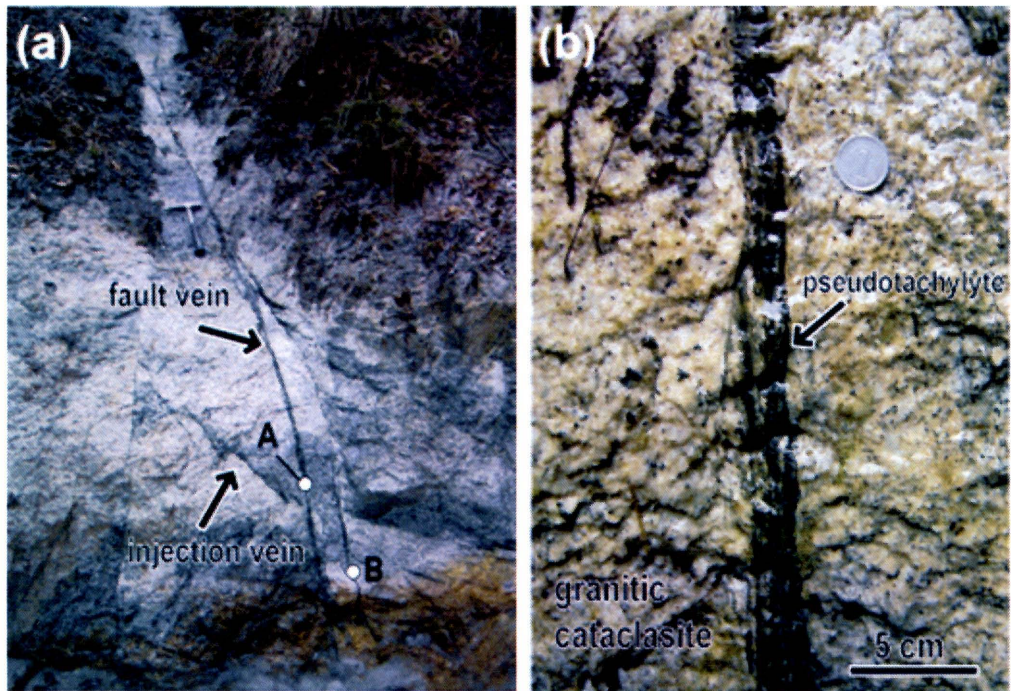
Fig. 1-2 Photographs of the field occurrence of Iida pseudotachylyte. (a) Pseudotachylyte occurring as black veins (arrow). The location of this outcrop is shown in Fig. 1-1. White circles indicate sampling points for XRF-EDS analyses. (b) Pseudotachylyte and granitic cataclasite.
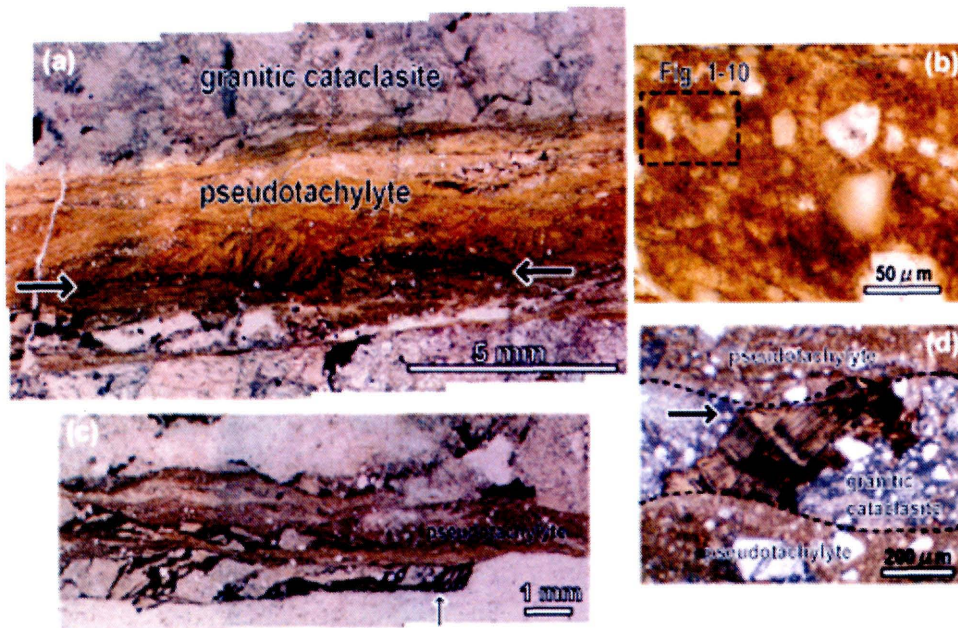
Fig. 1-3 Photomicrographs of the textures of Iida pseudotachylyte. (a) Thin dark-brown layers with flow structures. The texture formed by fluidization (arrow). PPL. (b) Fine-grained pale brown to dark brown matrix and angular fragments of quartz and feldspar. The outlined area indicates the field of view shown in Fig. 1-9. PPL. (c) Dark brown layers (deformed biotite) cut by a pseudotachylyte vein. PPL. (d) Biotite with kink bands cut by a pseudotachylyte vein (arrow). PPL.

66
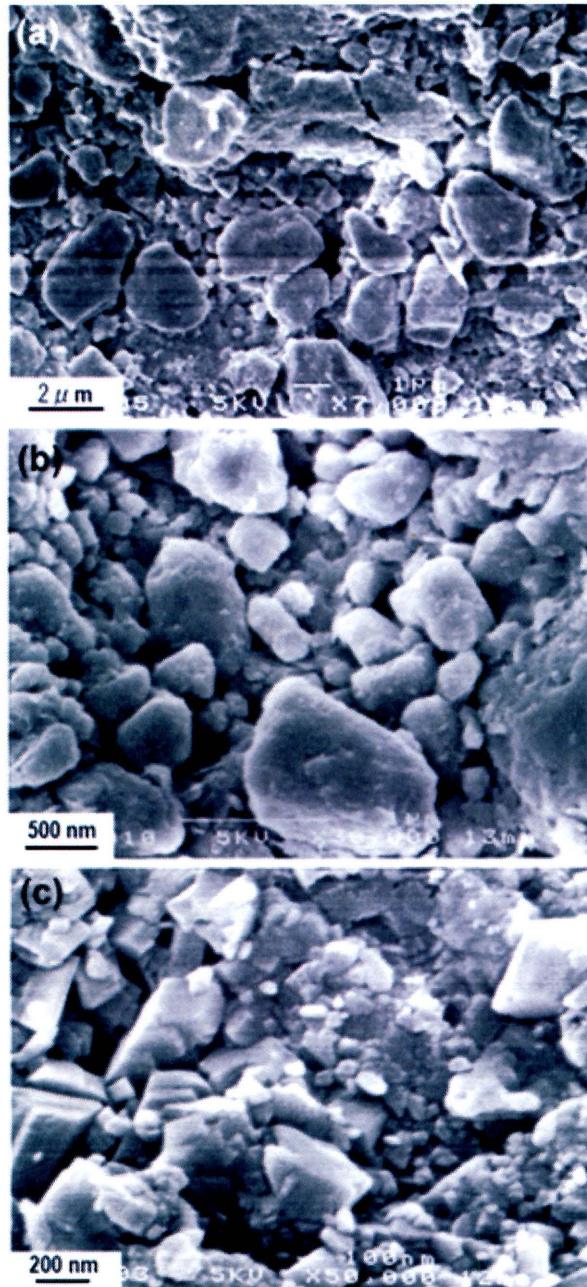
Fig. 1-4 HRSEM photomicrographs of textures on the breakage surfaces of Iida pseudotachylyte. (a) Angular to subangular fragments and extremely fine-grained matrix (x7000). (b) Pseudotachylyte matrix (x30000). (c) Fragments of several tens of nanometers in size exist within the Pseudotachylyte matrix (x50000).
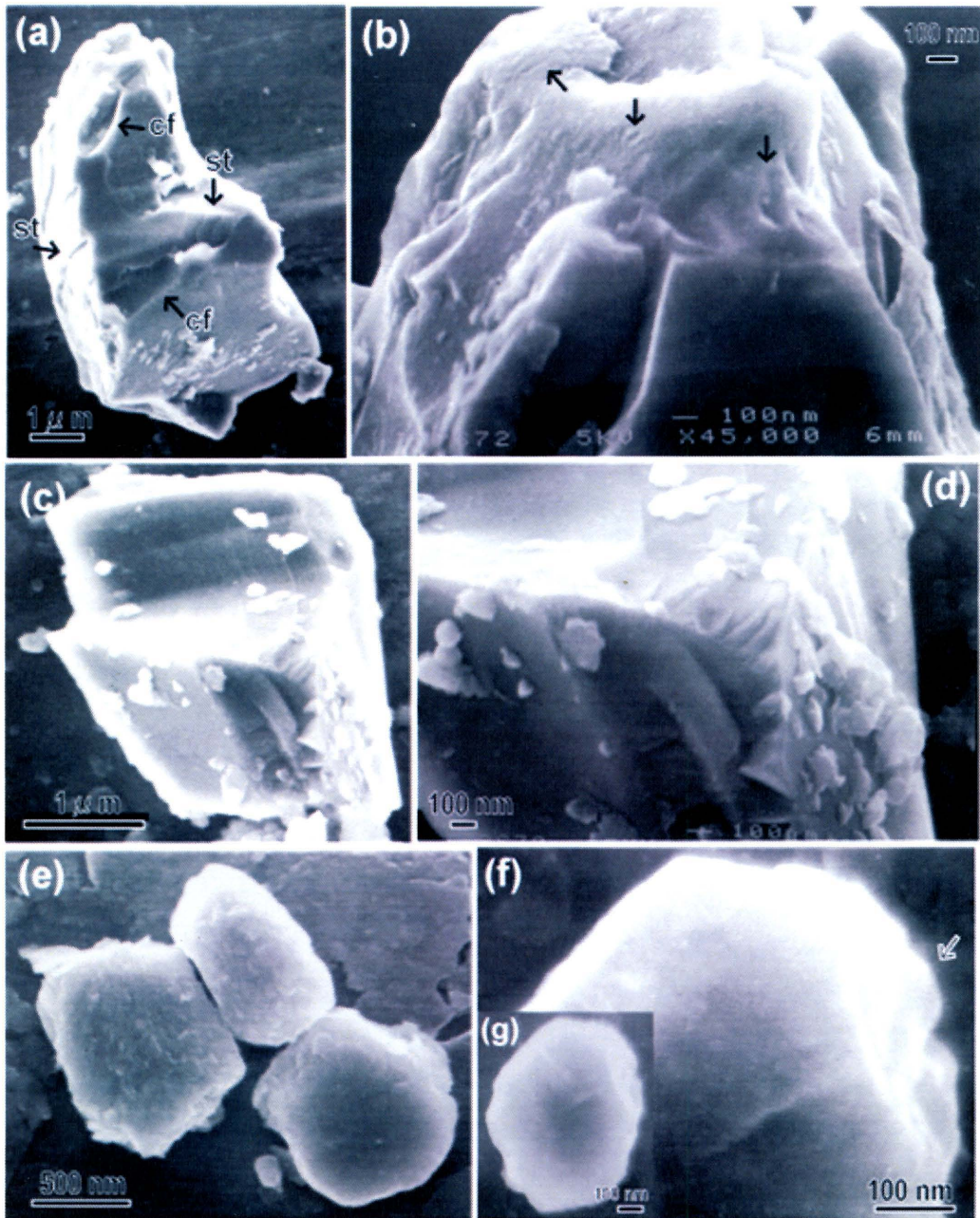
Fig. 1-5 HRSEM photomicrographs of the surface textures of fragments < 1 μm. (a) Angular fragment with conchoidal fractures (cf) and step-like textures (st). (b) Enlargement of the upper part of the fragment shown in (a). Arrows highlight many small scratches and holes. (c) Conchoidal fracture. (d) Step-like textures upon a conchoidal fracture surface. Enlargement of the central part of the fragment shown in (c). (e) Submicron fragments with relatively rounded shapes and slightly rough surfaces, similar to orange peel-like texture. (f) Enlargement of the upper right part of the fragment shown in (g). Submicron fragments with blunt edges similar to subconchoidal fracture (arrow).
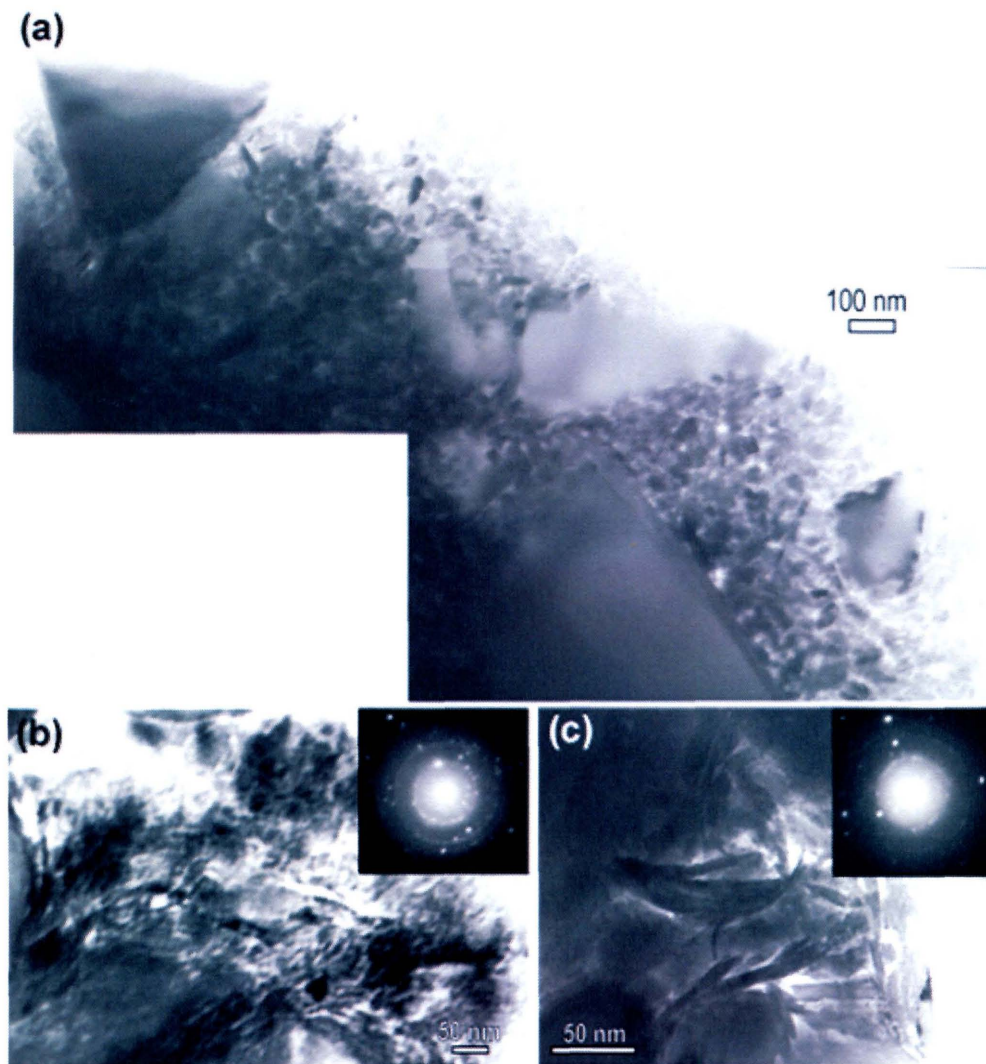
Fig. 1-6 TEM micrographs of bright-field (BF) images of the pseudotachylyte matrix obtained using 100 kV TEM. (a) Randomly orientated fragments that range in size from several tens of nanometers to a few micrometers. (b, c) Higher-magnification micrographs of a region of the pseudotachylyte matrix dominated by nanoscale particles smaller than 100 nm. Deformed elongated fragments are locally observed (c). Insets in (b) and (c) show the corresponding SAD patterns, showing the superimposition of diffuse ring patterns, ring patterns with biotite spacings, and diffraction spots. The SAD patterns were obtained with an aperture diameter of 500 nm.
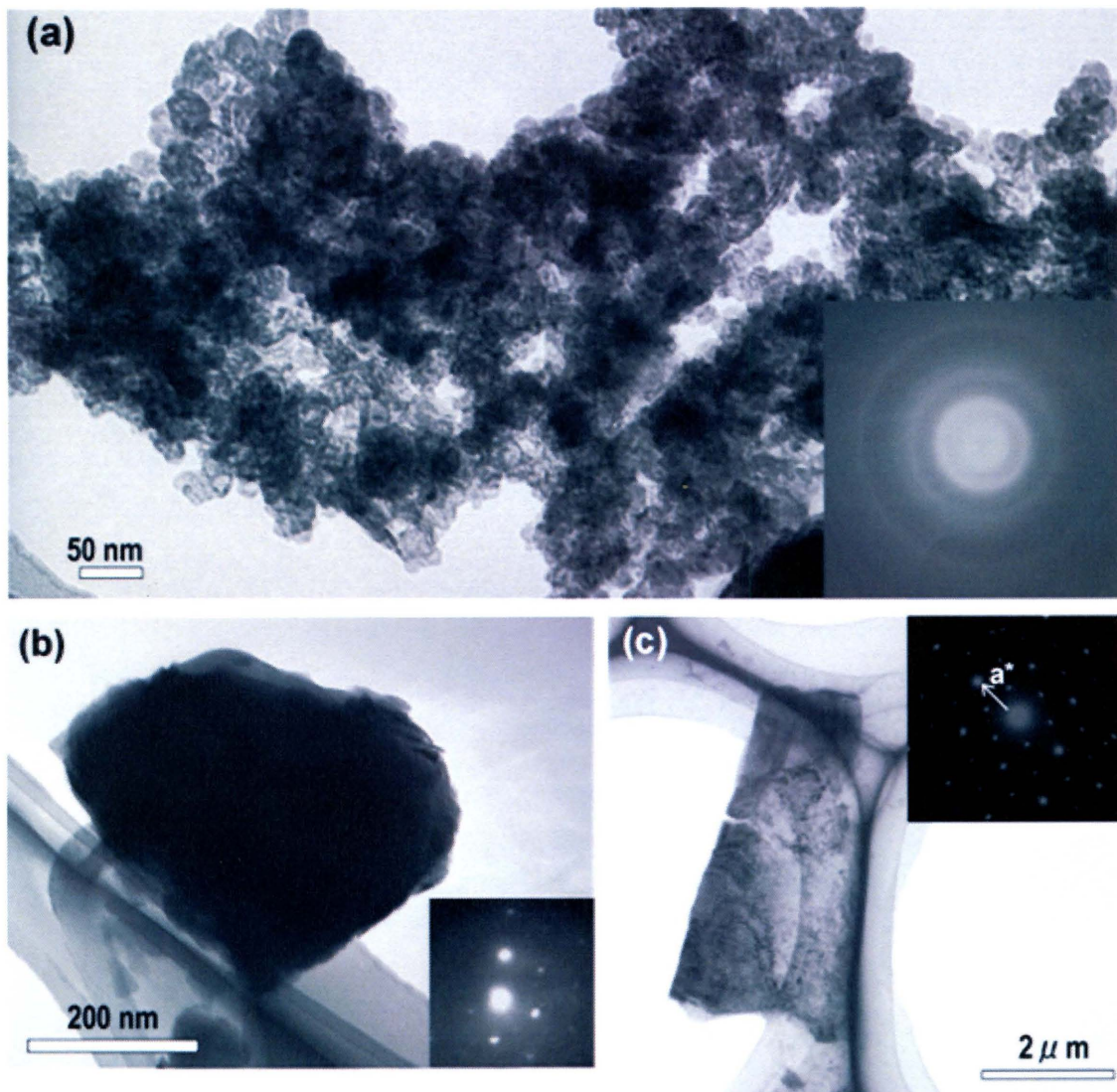
Fig.1-7 TEM micrographs of the particles of <1 μm in size in the pseudotachylyte matrix that were dispersed with ultrasonic agitation. (a) Agglomeration of nanoscale tabular particles. The inset shows the corresponding SAD pattern, which demonstrates diffuse ring patterns, indicating amorphous material. (b) Sub-rounded of several hundreds of nanometers in size show a single-crystal pattern by SAD. (c) TEM micrographs showing a BF image and SAD pattern of a biotite fragment sampled from the host rock. All SAD patterns were obtained with a diameter aperture of 500 nm.
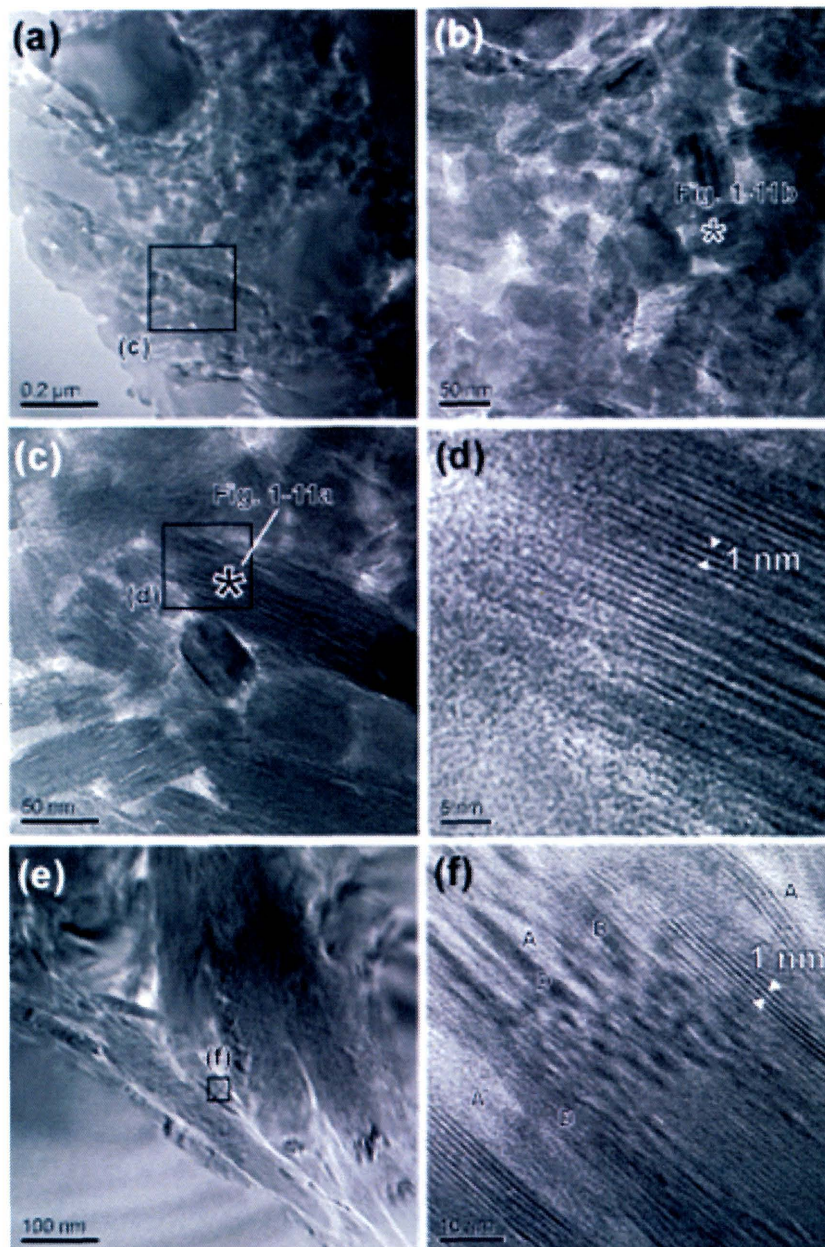
Fig. 1-8 HRTEM micrographs of the pseudotachylyte matrix. (a) BF image of the pseudotachylyte matrix. The outlined area indicates the field of view shown in (c). (b, c) BF images of an area consisting of nanoscale tabular particles with irregular shapes and elongated fragments. Asterisks represent the sites of qualitative EDS analyses (see Fig. 1-11). Both fragments have biotite conpositions. (d) Lattice fringe image of the area outlined in (c). (e) Bent and fractured elongated fragment. (f) Lattice fringe image of the area outlined in (e). Periodic lattice fringes with 1 nm spacing, corresponding to the (001) spacing of biotite, are indistinct and appear to lack periodicity, indicating lattice distortion (D) and the presence of an amorphous phase (A).

71
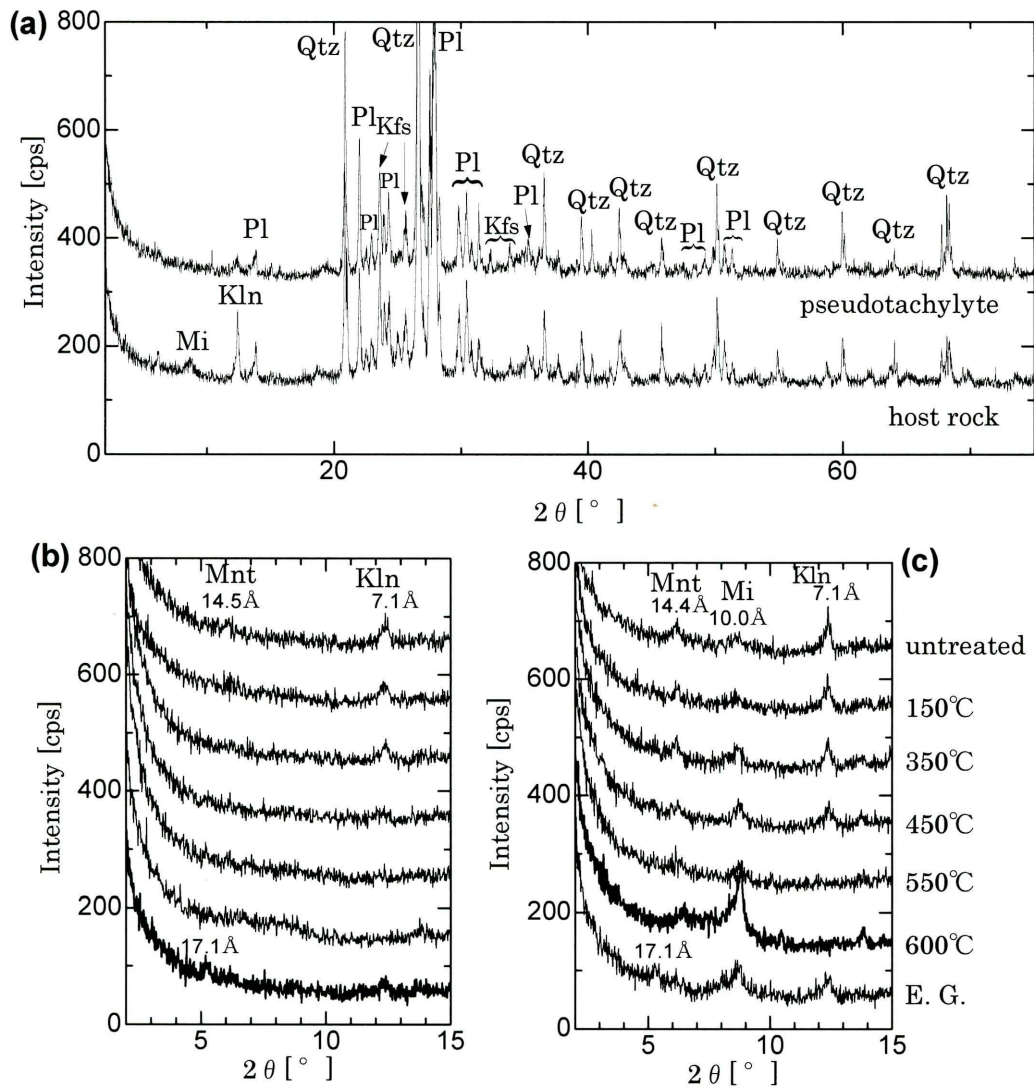
Fig. 1-9 X-ray diffraction patterns of pseudotachylyte and host rock (granitic cataclasite). (a) Spectra of the main minerals. (b, c) Spectra of clay minerals detected in the hydraulically elutriated samples. (b) Pseudotachylyte. (c) Host rock. 150, 350, 450, 550, and 600 °C : heated at the given temperature for 1 hour. E.G.: treated with ethylene glicol. Qtz: quartz, Pl: plagioclase, Kfs: K-feldspar, Mnt: montmorillonite, Mi: mica clay mineral, Kln: kaolinite.
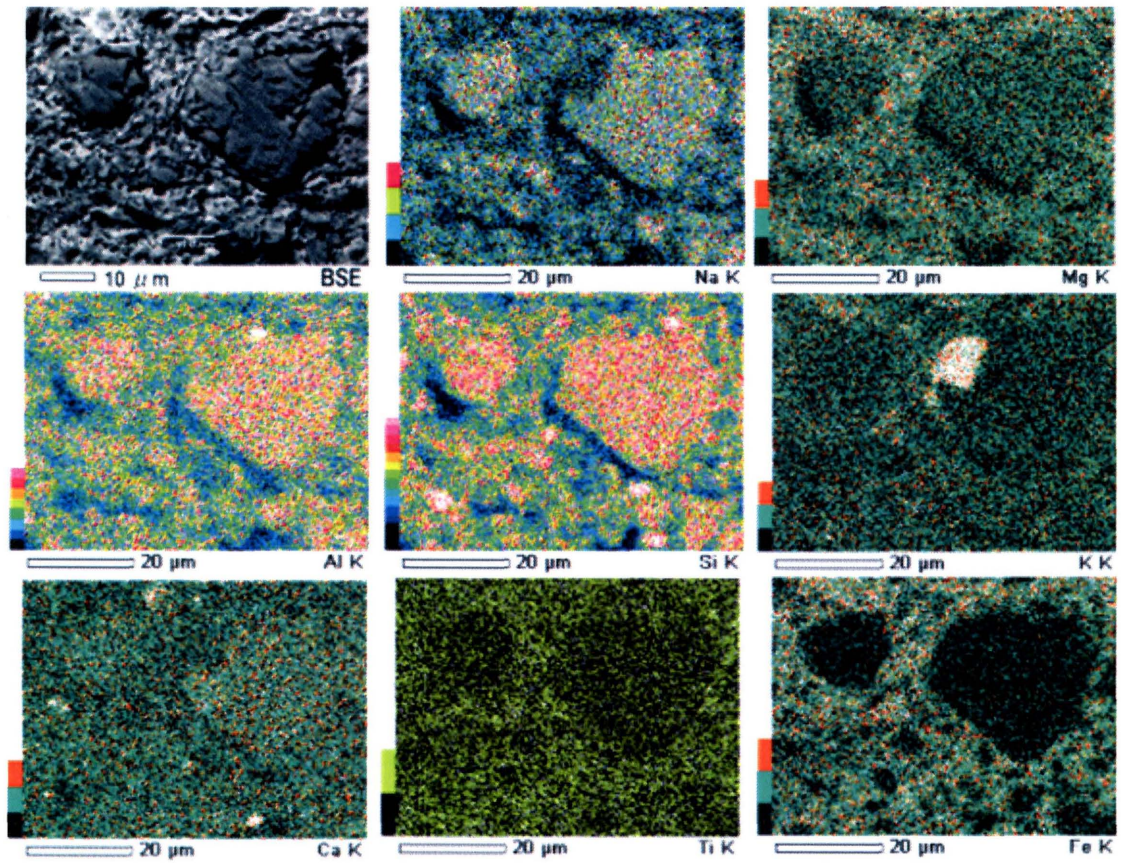
Fig.1-10 Backscattered electron (BSE) micrograph and SEM-EDS elemental maps showing the distributions of Na, Mg, Al, Si, K, Ca, Ti, and Fe in the Iida pseudotachylyte. Note that the matrix is enriched in Fe, Mg, K, and Ti. BSE and mapping images were taken of the area outlined in Fig. 1-3b.
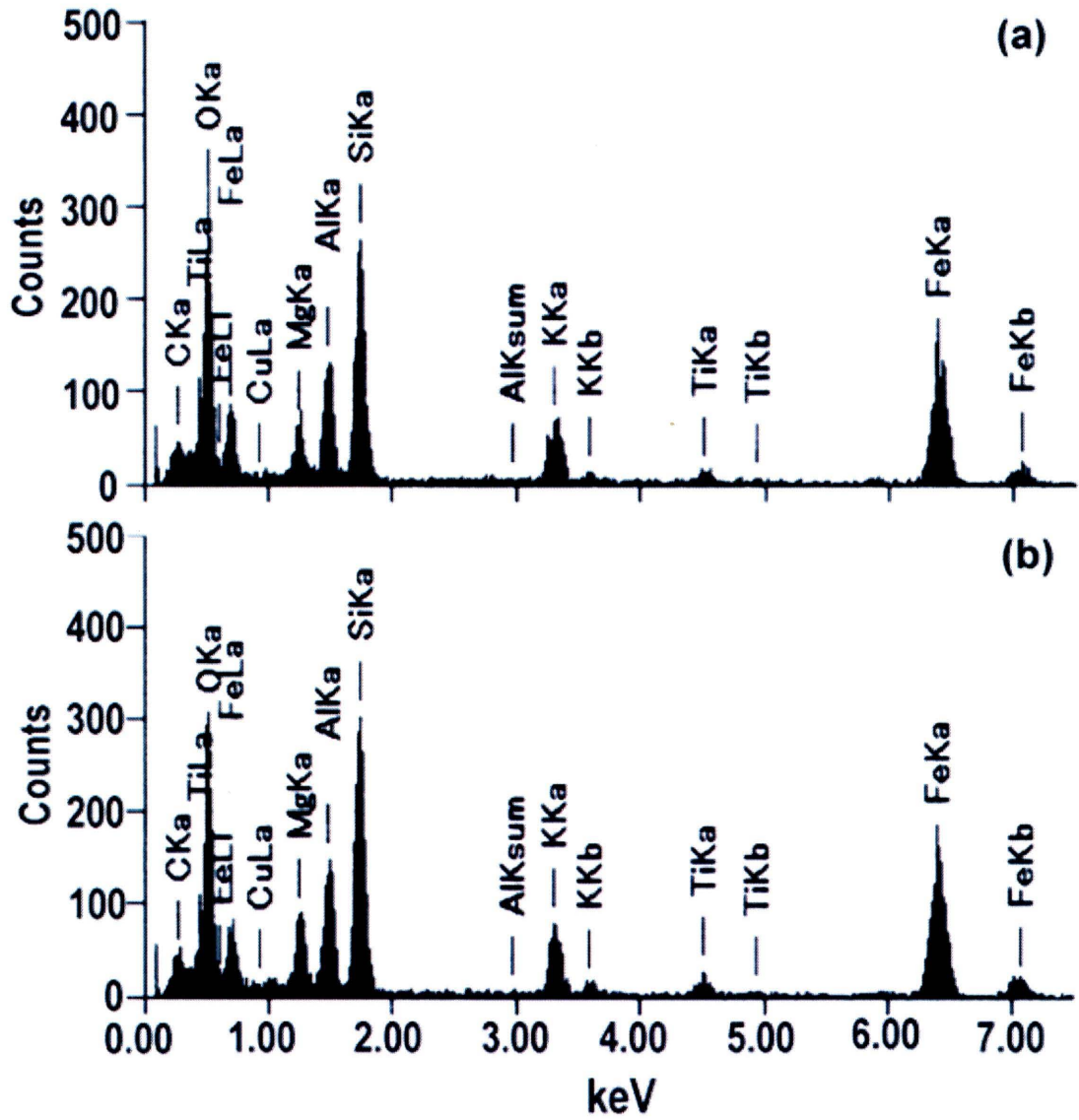
Fig. 1-11 TEM-EDS spectra of elongated fragments (a) and a nanoscale tabular particle (b) in the pseudotachylyte matrix. The small C peaks in both spectra are due to carbon-coating. The sites of analyzed points are shown by asterisks in Fig. 1-8b, c.

74
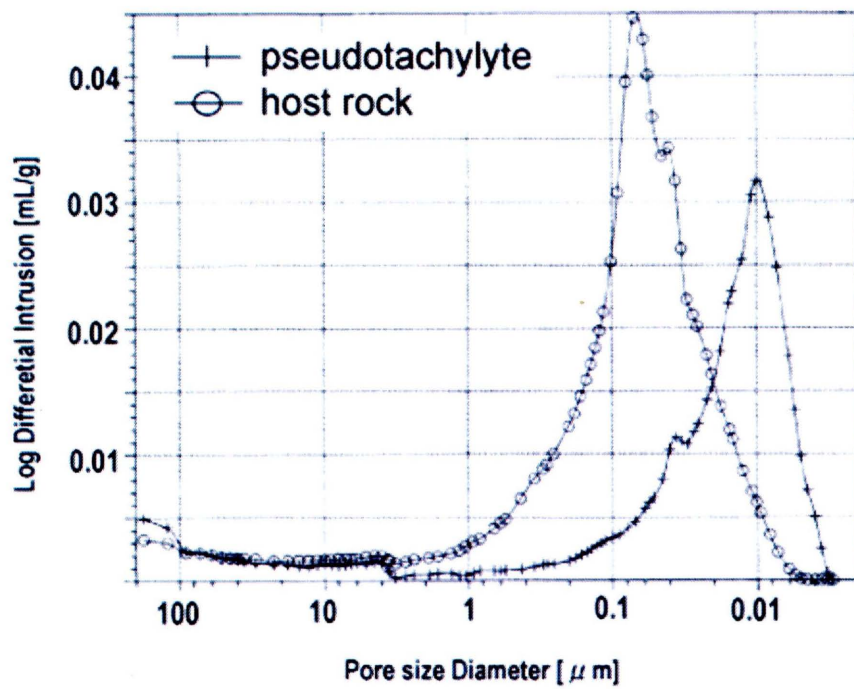
Fig. 1-12 Pore-size distributions of pseudotachylyte and host rock. Note that the host rock is more porous than the pseudotachylyte.
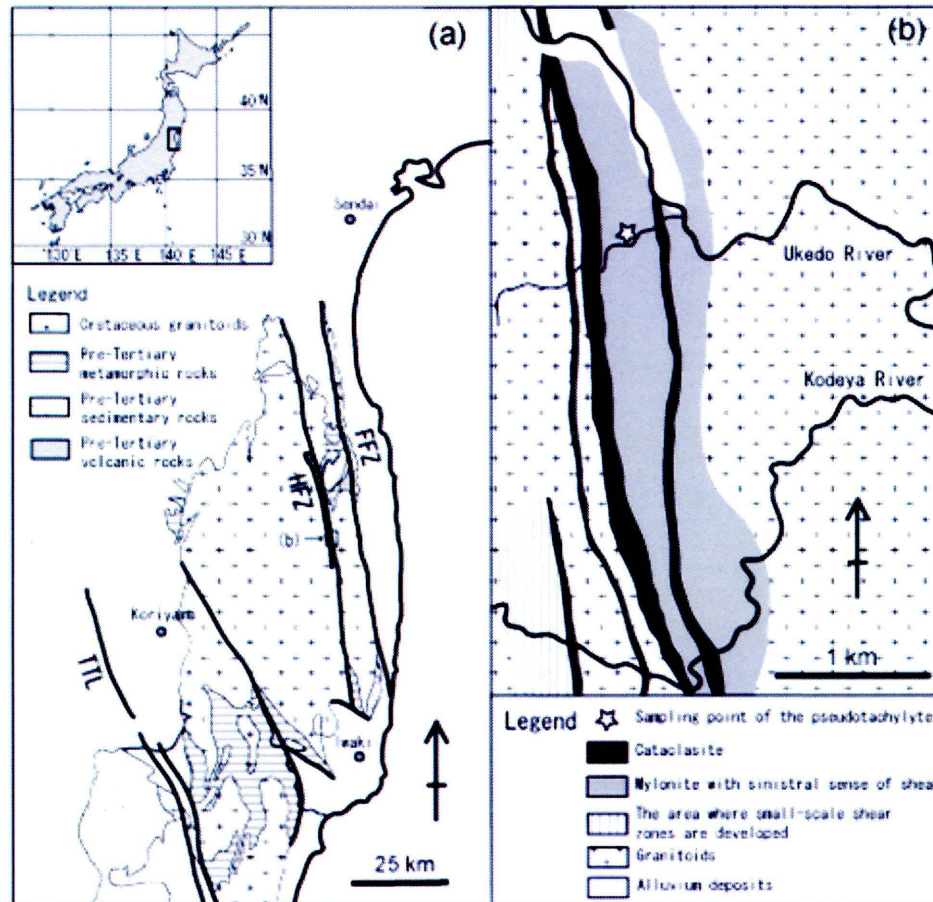
Fig. 2-1 Location of the Hatagawa Fault Zone and outcrops. (a) Geologic map of the Hatagawa Fault Zone (additions based on Kubo *et al*., 1990, and Shigematsu *et al*., 2003). FFZ: Futaba Fault Zone, HFZ: Hatagawa Fault Zone, and TTL: Tanakura Tectonic Line. (b) Lithofacies map of the outcrops as sampling sites (additions based on Shigematsu and Yamagishi, 2002, and Shigematsu *et al*., 2003).
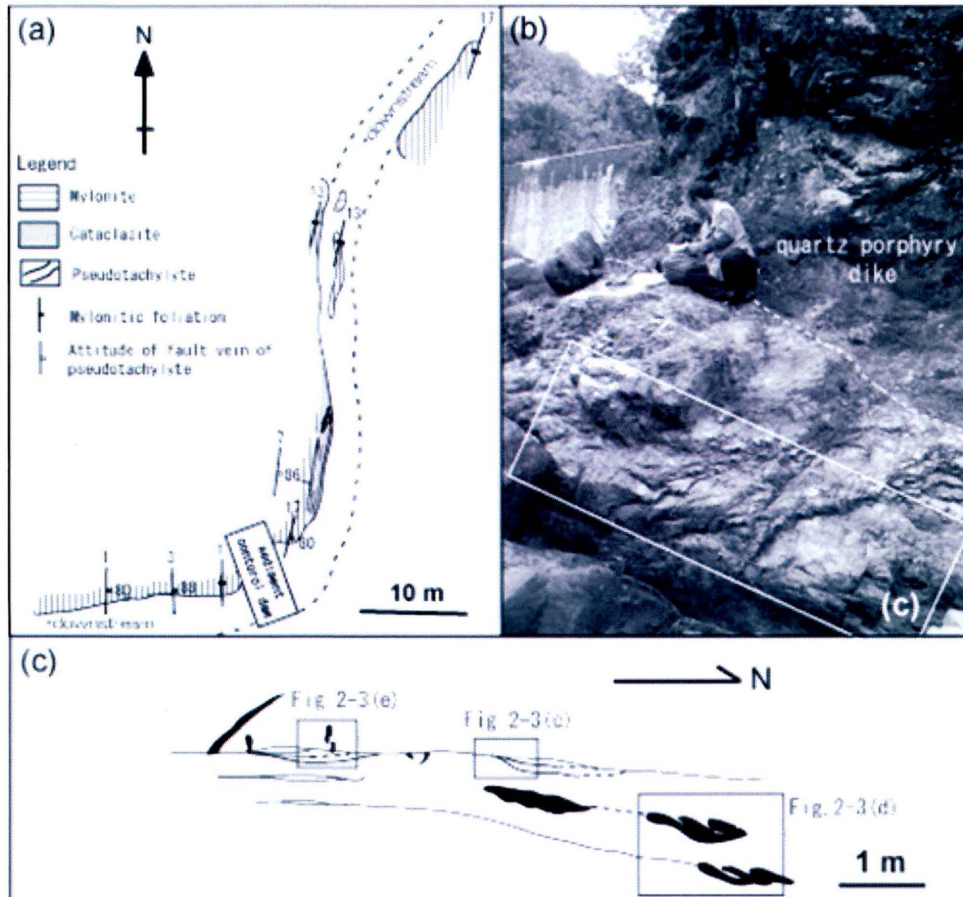
Fig. 2-2 (a) Lithofacies map of the outcrop producing pseudotachylyte. (b) Entire view of the outcrop. (c) Sketch of the occurrence of pseudotachylyte (boxed in b).
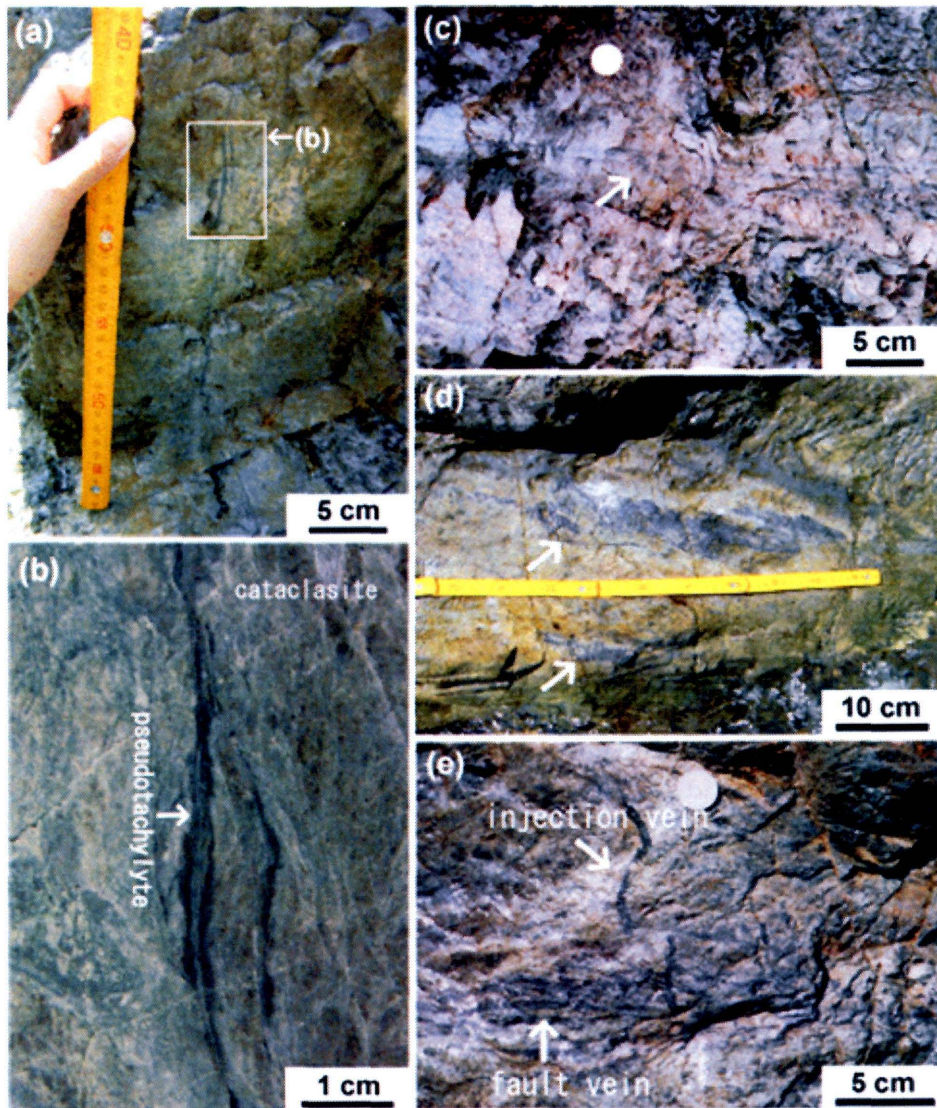
Fig. 2-3 Features of the pseudotachylyte outcrop. (a) Dark-green-veined pseudotachylyte (boxed). (b) Polished surface of the box in a. A clear boundary with the host rock is shown. (c) Branching fault vein (branching to the right starts at the arrow). (d) Fractured fault veins (arrows). (e) Left-lateral injection vein affected by a small fault. Figures c through e are the photos of the parts respectively shown in Fig. 2-2c.
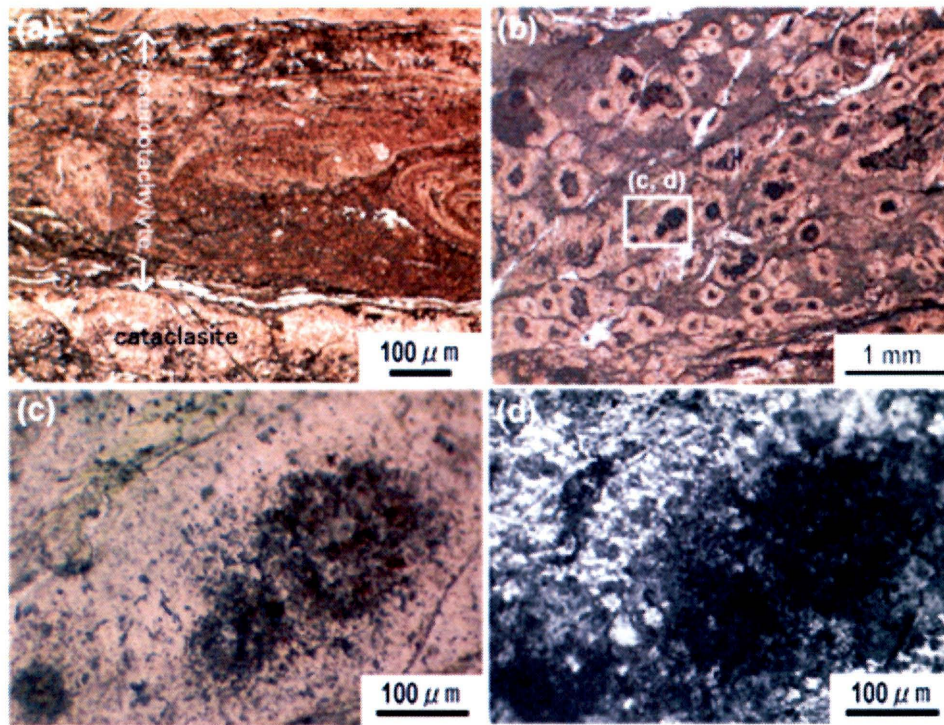
Fig. 2-4 Photomicrographs of the pseudotachylyte thin section. (a) Pseudotachylyte fault vein cutting the cataclasite. plane polarized light (PPL). (b) Spherulite formed in the matrix of the fault vein (PPL). (c) Enlargement of box in b (PPL). (d) Recrystallized texture formed inside the spherulite. Cross-polarized light of c.
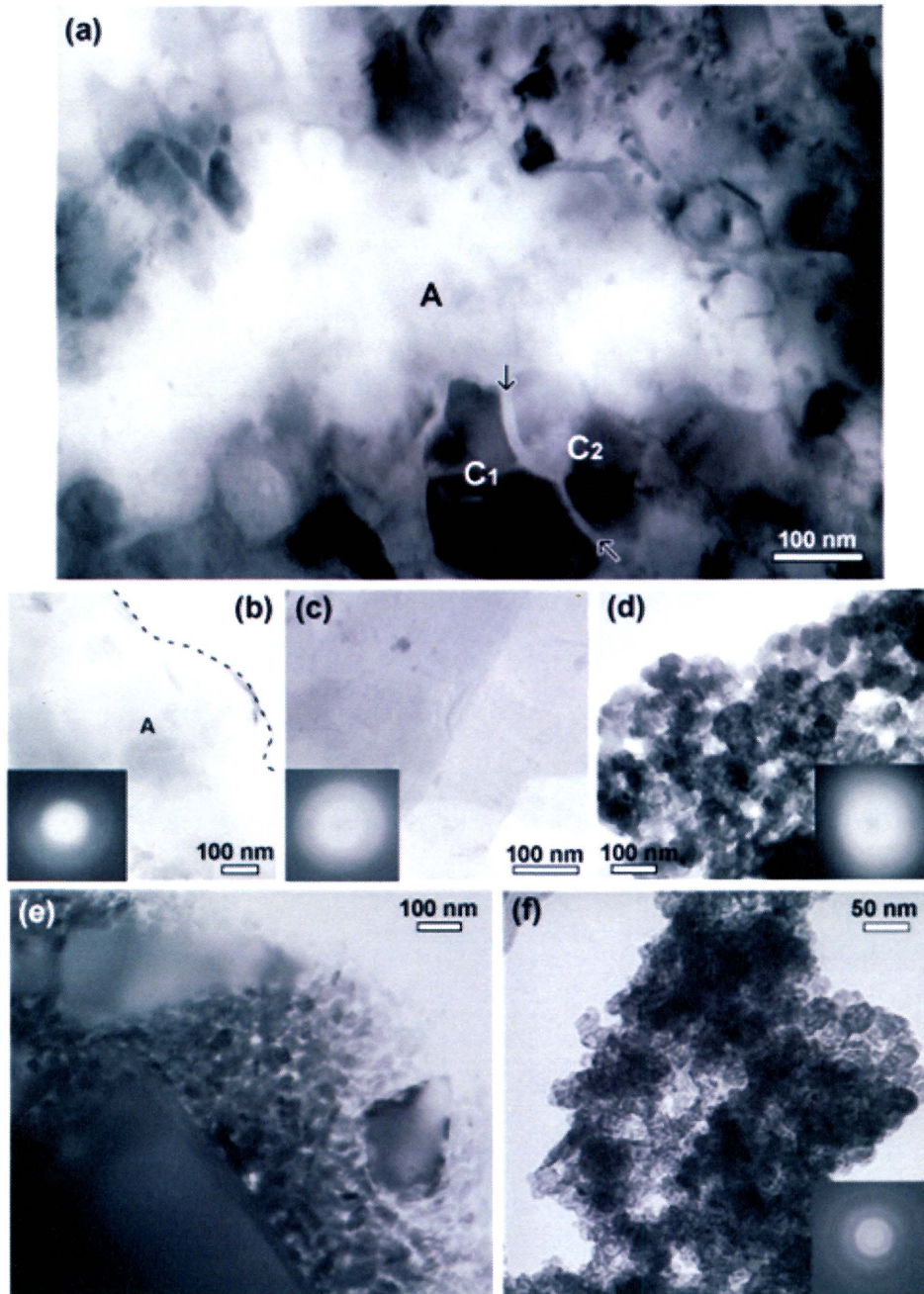
Fig. 2-5 TEM photo (bright-field image) and selected-area electron diffraction images (inserts; irradiation diameter 500 nm). (a) Amorphous material of melt-origin (A) contained in the pseudotachylyte of the Hatagawa Fault Zone. The arrow points to amorphous material injection between crystal grains C1 and C2. The boundary between C1 and the amorphous material is clear. (b) Amorphous material of melt-origin (A, below dashed line) in the pseudotachylyte of the Hatagawa Fault Zone. (Area above dotted line is empty.) (c) Amorphous material formed in melting test. (d) Amorphous material formed by comminution in low-speed shear test. (e, f) Amorphous material of crush-origin in the pseudotachylyte of the Iida–Matsukawa Fault. (a, e: prepared by ion milling; b, c, d, f: prepared by crushing).
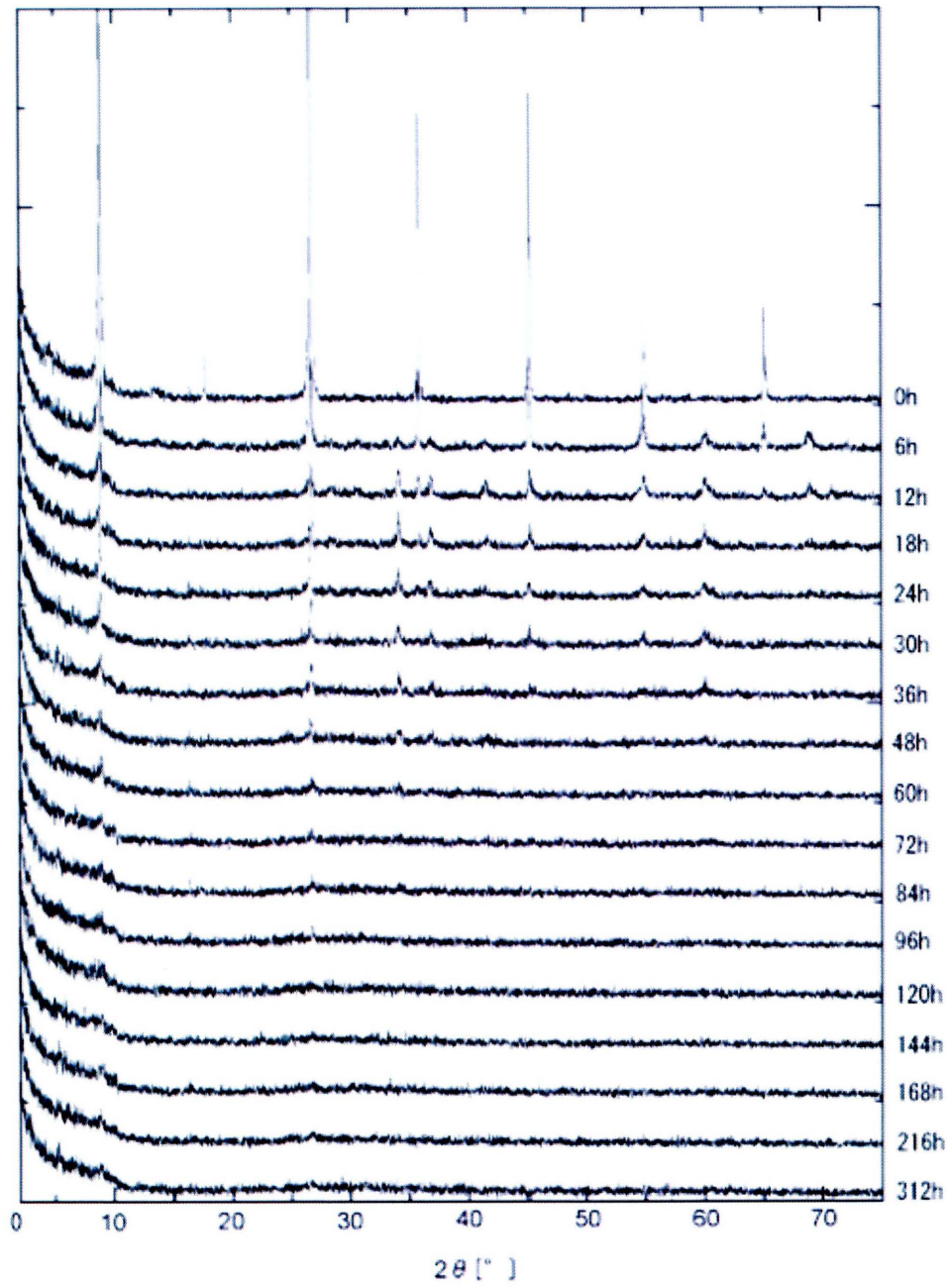
Fig.3.1. X-ray diffraction patterns of comminuted particles. Numbers shown at the right of the figure are mean grinding times (h: hours).
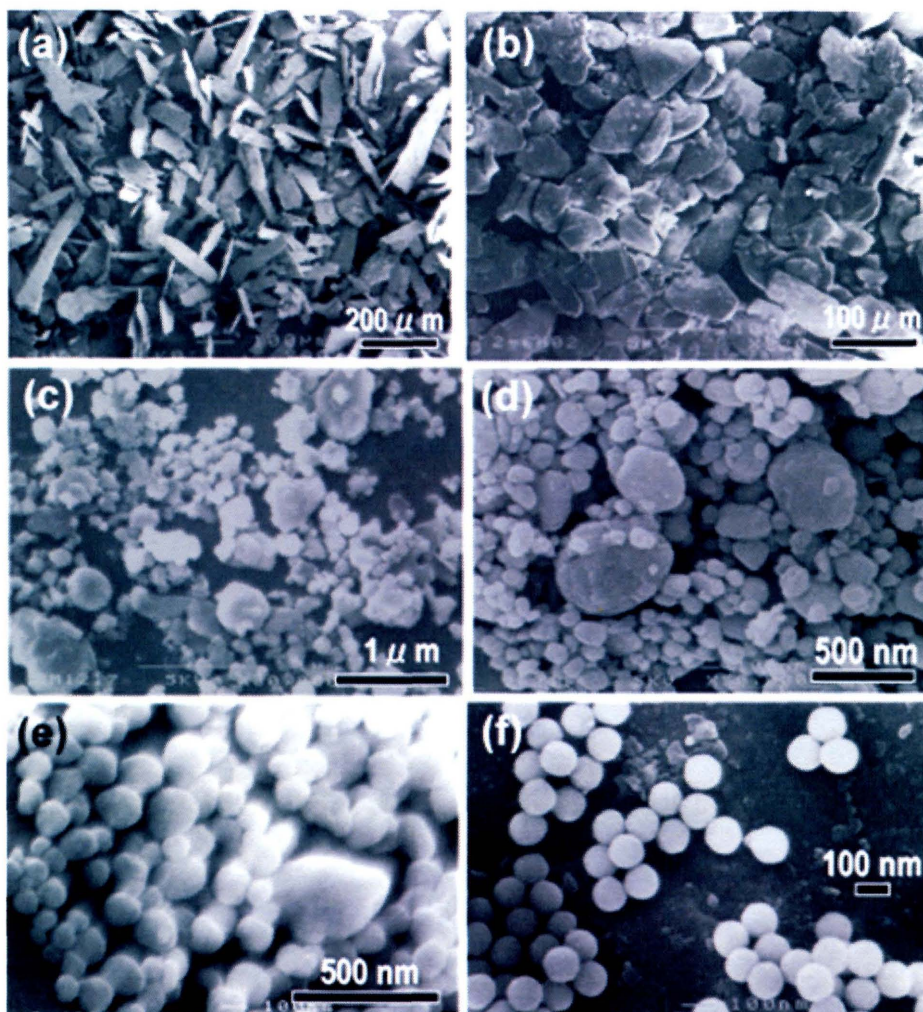
Fig.3-2 X-ray diffraction patterns of comminuted particles. (a) starting material; (b) ground for 6 h; (c) ground for 12 h; (d) ground for 24 h; (e) ground for 48 h; (f) ground for 312 h
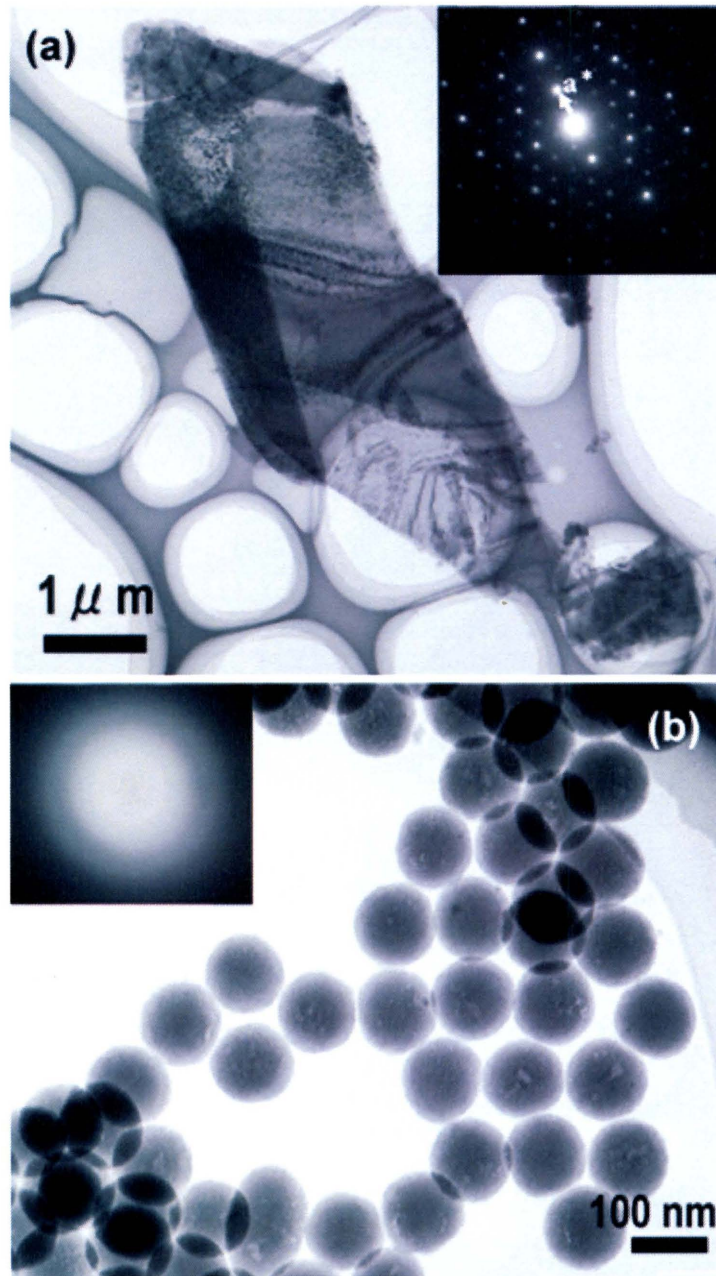
Fig.3-3 TEM micrographs of bright-field images and selected-area diffraction (SAD) patterns. (a) Starting material with platy shape. Inset is the SAD pattern of a single-crystal. (b) ground for312 hours samples with spherical shapes. Inset is the SAD pattern of the spherical particles of amorphous materials. All SAD patterns were obtained with a diameter aperture of 500 nm.
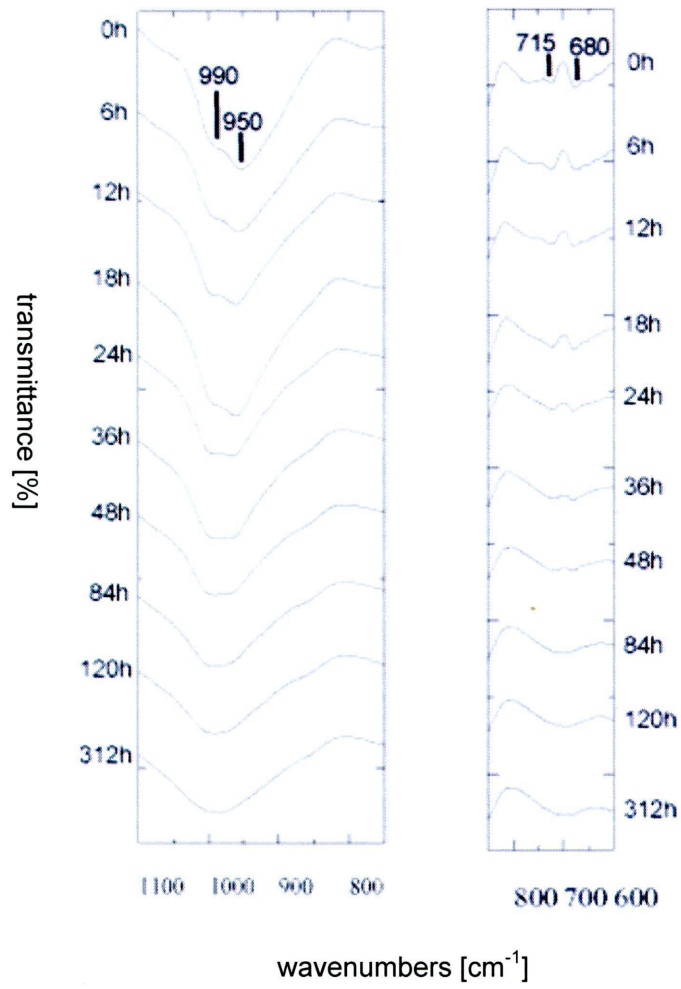
Fig.3-4 Infrared absorption spectra of comminuted particles. Numbers shown next to figures are grinding times (h: hours).
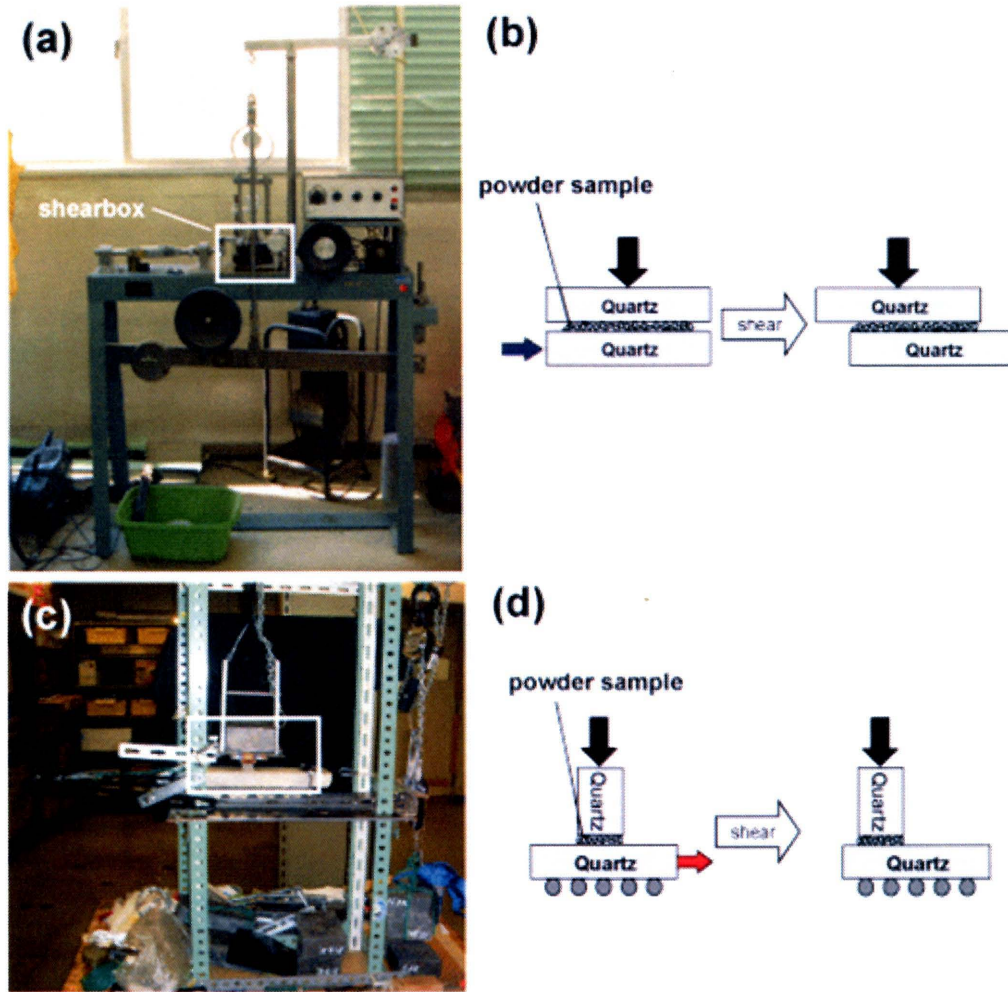
Fig. 4-1 Photos and diagrams of apparatuses used for the sliding shear tests. (a) The direct-shear apparatus used for the low-speed shear tests. Shearbox at the center of the apparatus. (b) Diagram of shearbox in the direct-shear apparatus used for the low-speed shear test. (c) The shear apparatus used for the high-speed shear tests. The shear plane is at the center of this photo. (d) Diagram of the area outlined in (c), which includes the shear plane under high-speed shear conditions.
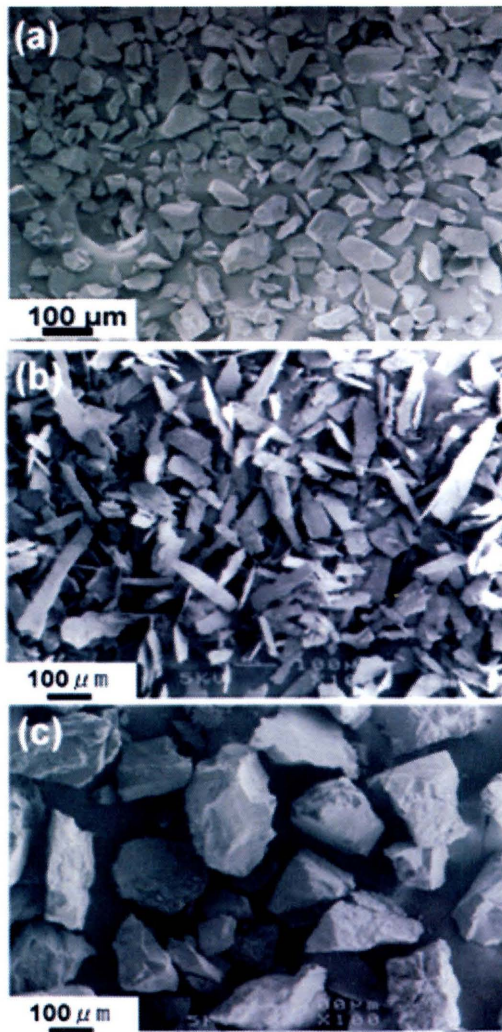
Fig.4-2 SEM photomicrographs of starting materials. (a) quartz (b) biotite, and (c) granite cataclasite samples of the host rock obtained from the pseudotachylytes of the Iida–Matsukawa fault.
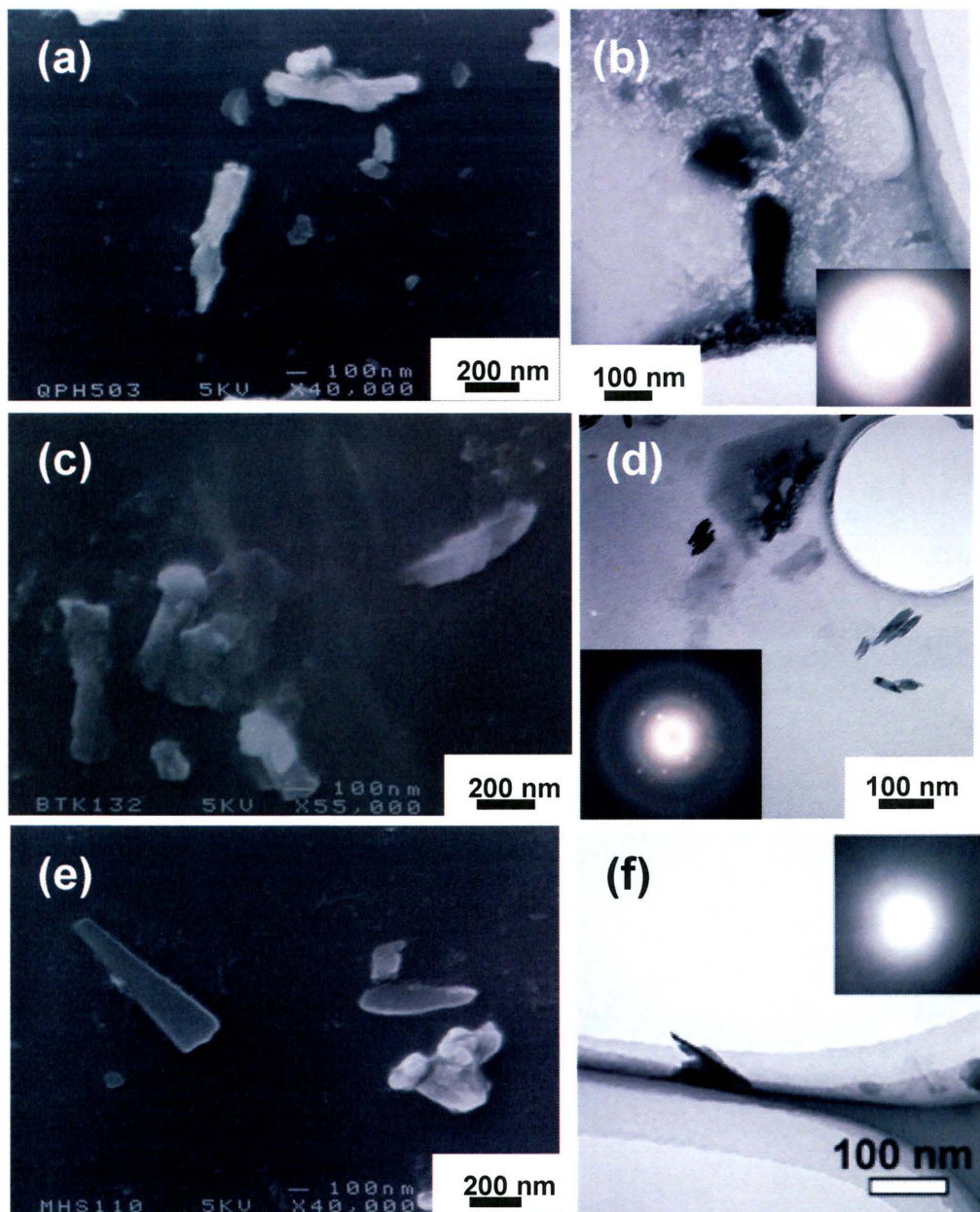
Fig.4-3 SEM and TEM photomicrographs showing the elongated submicron particles were formed at a high slip rate. (a, b) quartz (c,d) biotite (e,f) granite. a,c,and e are SEM images. b,d, and f are TEM images and selected area diffraction patterns.
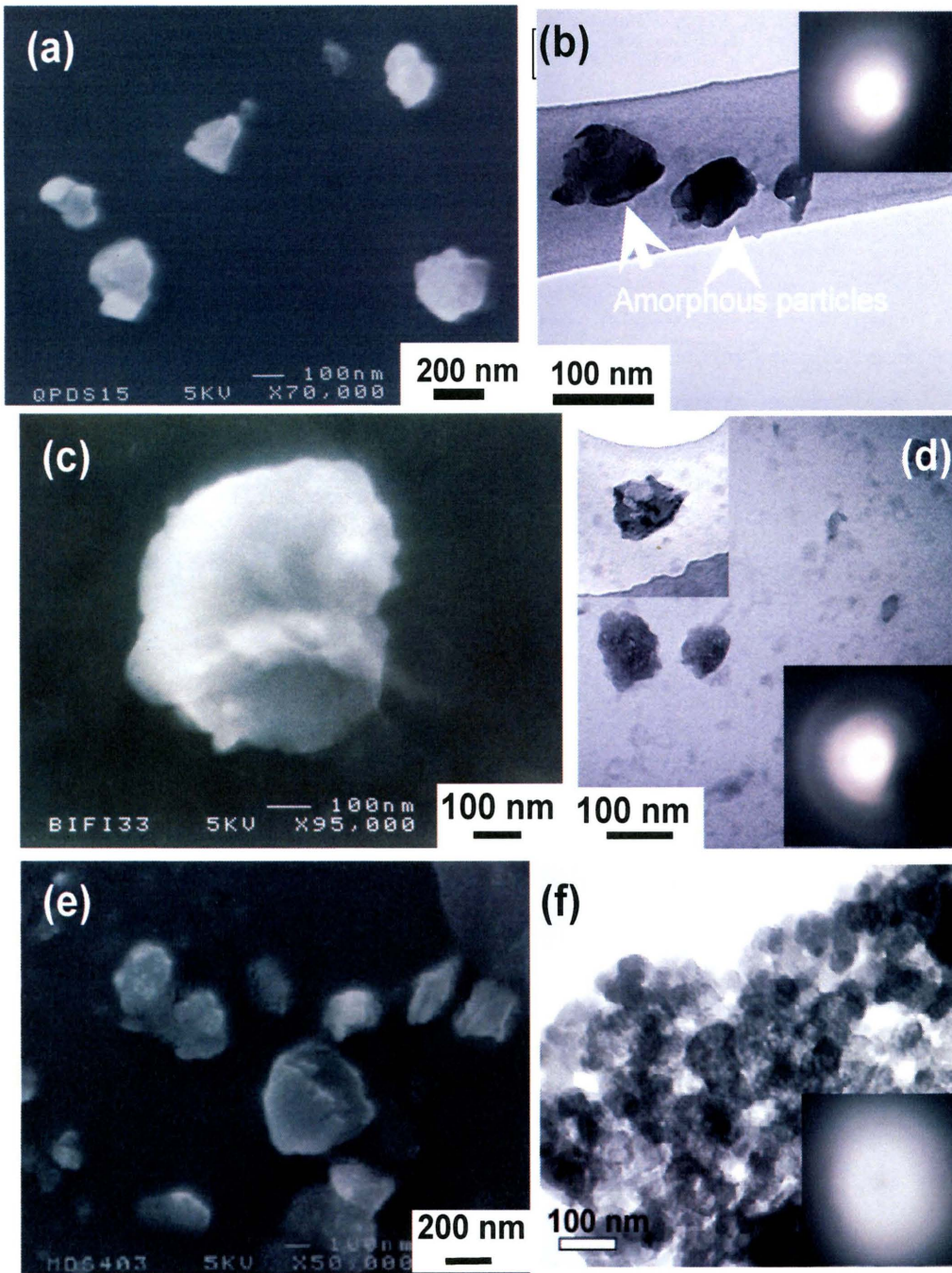
Fig.4-4 SEM and TEM photomicrographs showing the polygonal or spherical submicron particles were formed at a low slip rate. (a, b) quartz (c,d) biotite (e,f) granite. a, c, and e are SEM images. b, d, and f are TEM images and selected area diffraction patterns.
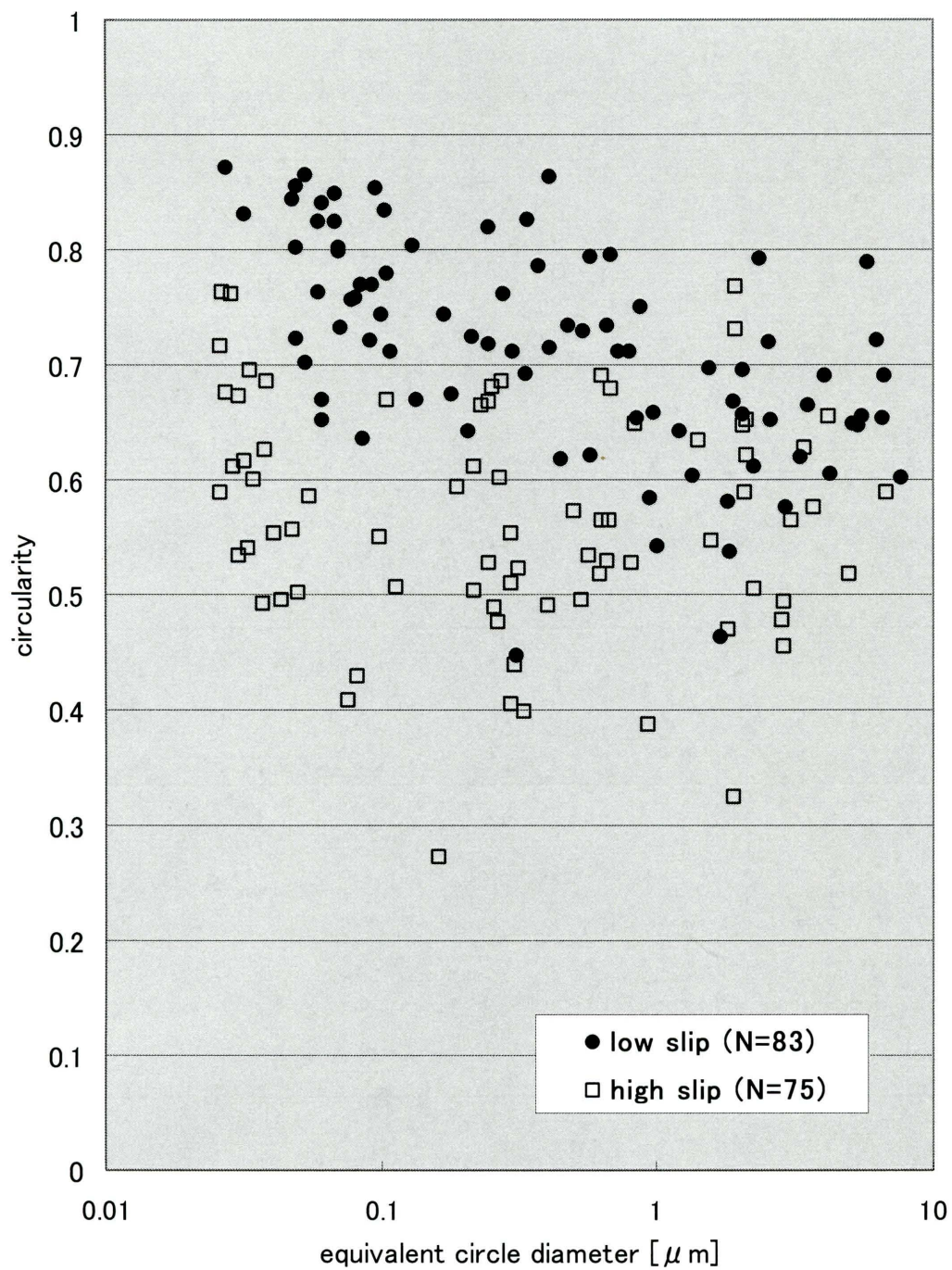
Fig. 4-5 Relationship between equivalent circle diameter and circularity of comminuted biotite particles after shear slip tests.
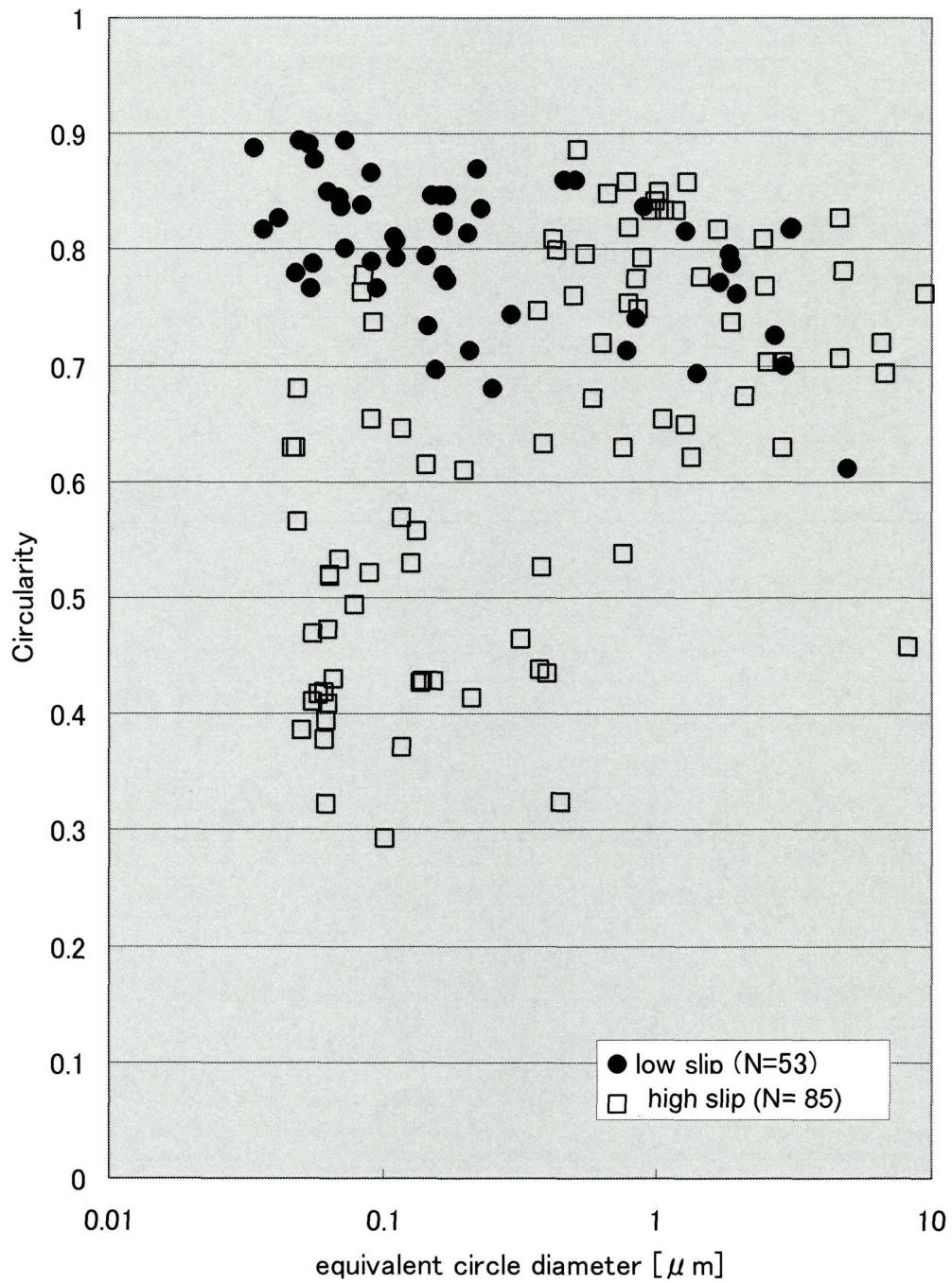
Fig. 4-6 Relationship between equivalent circle diameter and circularity of comminuted quartz particles after shear slip tests.
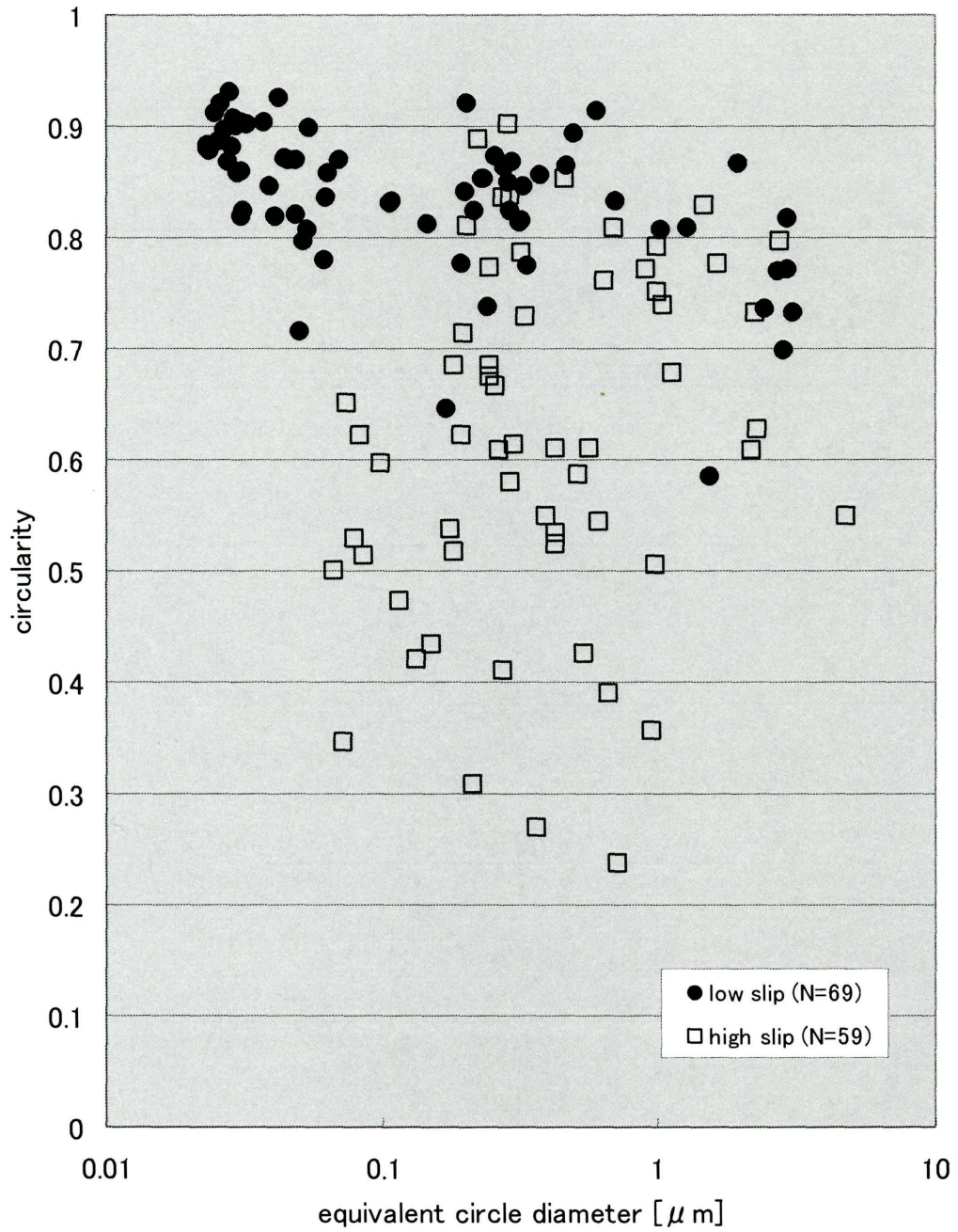
Fig. 4-7 Relationship between equivalent circle diameter and circularity of comminuted granite cataclasite (host rock of the Iida-Matsukawa pseudotachylyte) particles after shear slip tests.
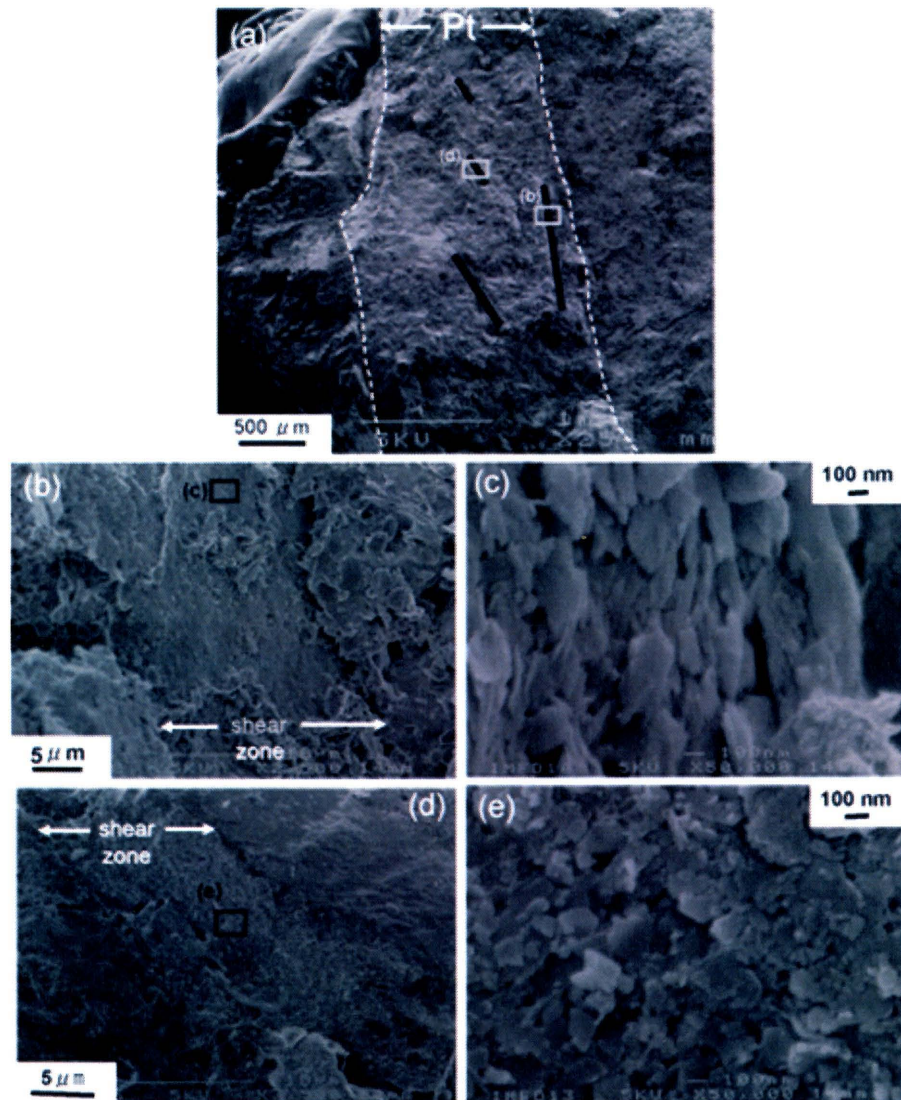
Fig.4-8 (a) SEM photomicrograph of freeze-dried breakage surface of the Iida–Matsukawa pseudotachylyte. Pt: pseudotachylyte. (b) Higher magnification micrograph of parallel shear surfaces of the pseudotachylyte vein. (c) Assembly of elongated particles on the parallel shear surfaces: enlargement of center area of the area outlined in (b). (d) Higher magnification micrograph of oblique shear surfaces of the pseudotachylyte. Image area is the area outlined in (a). (e) Assembly of polygonal or nearly spherical particles on oblique shear surfaces. Enlargement of upper area of the area outlined in (d).

Table 1-1 Bulk compositions of host rock and pseudotachylyte, as determined by XRF-EDS. All values are normalized to 100% totals. The locations of sampling points are shown in Fig. 1-2a.

wt%	host rock	pseudotachylytes			
		A-1	A-2	B-1	B-2
SiO_2	73.14	68.83	68.84	68.60	68.69
TiO_2	0.15	0.57	0.58	0.64	0.65
Al_2O_3	13.39	13.55	13.56	13.54	13.60
Fe_2O_3	1.20	5.69	5.62	5.89	5.84
MnO	0.03	0.15	0.16	0.12	0.12
MgO	0.03	0.71	0.84	0.88	1.02
CaO	1.34	2.66	2.64	2.63	2.60
Na_2O	3.06	4.03	3.93	4.31	4.17
K_2O	7.35	3.31	3.34	2.84	2.80
P_2O_5	0.30	0.51	0.49	0.55	0.51